The Hong Kong Polytechnic University

Department of Civil and Structural Engineering

Thesis entitled

"The photocatalytic degradation of alachlor and dicamba in TiO_2 suspension"

submitted by

Wong Chi Chung

A thesis submitted in partial fulfillment of the requirements for the degree of Master of Philosophy in Environmental Engineering

September 2003

CERTIFICATE OF ORIGINALITY

I hereby declare that this thesis is my own work and that, to the best of my knowledge and belief, it reproduces no material previously published or written nor material which has been accepted for the award of any other degree or diploma, except where due acknowledgement has been made in the text.

_____(Signed)

Wang Chi Chung (Name of student)

Abstract

Direct photolysis and photocatalytic degradations of two widely used herbicides: alachlor and dicamba were studied using three different monochromatic UV lamps (254 nm, 300 nm and 350 nm). The photocatalytic reactions were studied under various conditions including the examination of the effects of different TiO_2 sources, TiO_2 dosages, initial pH and proton sources. The influence of the addition of hydrogen peroxide in photocatalysis of alachlor and dicamba was also investigated using the UV at 300 and 350 nm. Degradation mechanisms of alachlor were studied through intermediates identification.

Both the direct photolysis and photocatalytic degradations of alachlor and dicamba follow pseudo first-order decay kinetics. Direct photolysis was a rather slow process, but the rate constants for alachlor photocatalysis were increased by about 11 and 26 times at 300 and 350 nm respectively, whereas the rate constants for dicamba photocatalysis were increased by about 3 and 5 times.

TiO_2-P25 was found to be an effective photocatalyst compared to TiO_2-BDH. The direct photolysis of alachlor and dicamba was dominant at 254 nm even if TiO_2 was present in the solution. Among the three UV wavelengths used, the highest photocatalysis quantum yield was obtained at 300 nm. The photocatalytic degradation rate of alachlor and dicamba increased with the dosages of TiO_2, but an overdose of TiO_2 would retard the reaction due to light attenuation. Photocatalysis rate of alachlor were slightly enhanced in an alkaline medium, and the different proton sources

causing various degrees of rate retardation were due to the presence of the corresponding counter anions.

At low to medium pH ranges, photocatalysis rate of dicamba were increased with pH because of the increase of hydroxide ions, but the reaction was gradually retarded at alkaline medium when the effect of charges repulsion was dominant. Rate retardation caused by the presence of the corresponding counter anions was also observed.

Photocatalytic degradations of alachlor and dicamba in TiO_2 suspensions with and without the use of hydrogen peroxide were studied using two different monochromatic UV irradiations (300 and 350 nm). The results of H_2O_2 assisted photocatalysis experiments showed that a low H_2O_2 dosage in photocatalysis using UV at 300 nm would enhance the pseudo first order decay rates by 3.3 times for alachlor and 2.4 times for dicamba, but overdose of H_2O_2 will retard the rate because of the expenditure of hydroxyl radicals. However, this process was found impracticable at UV 350 nm due to the absorption characteristic of H_2O_2.

In photocatalysis or H_2O_2-assisted photocatalysis of alachlor, a total of thirteen major intermediates were successfully identified using Liquid chromatography-electrospray ionization-mass spectrometry (LC-ESI-MS) and MS/MS. The major degradation mechanisms of alachlor photocatalysis include dechlorination, dealkylation, hydroxylation, scission of C-O bond, cyclization and N-dealkylation. Bell-shaped evolution profiles of different intermediates were observed. Accordingly, the degradation pathways of alachlor photocatalysis were proposed in relation to the intermediates evolution profiles to successfully illustrate series of degradation steps.

Acknowledgement

First of all, I would like to express my gratitude to:

Dr. W. Chu, my chief supervisor and associate Professor in the Department of Civil and Structural Engineering at The Hong Kong Polytechnic University, for his encouragement and valuable guidance.

Besides, I would like to thank the following scholars for their valuable comment and suggestion.

Dr. H. Chua, chairman of Board of Examiners and Professor in the Department of Civil and Structural Engineering at The Hong Kong Polytechnic University.

Dr. Irene M. C. Lo, external examiner and associate Professor in Department of Civil Engineering at The Hong Kong University of Science and Technology.

Dr. C. N. Chang, external examiner and Professor in Department of Environmental Science at The Taiwan Tunghai University.

Table of content

List of Tables

List of Figures

Chapter 1: Introduction

1.1 Advanced oxidation processes (AOPs)

Biological treatment of domestic wastewater has been used all over the world because of its cost effectiveness and versatility in handling a variety of organic pollutants. However, biological treatment has its difficulty to be operated when there are toxic and refractory chemicals in the wastewater (Tang and An, 1995). In such cases, a potentially useful approach is to partially pretreat the toxic waste by oxidation technologies to produce intermediates that are more readily biodegradable. As shown in Figure 1.1, many advanced oxidation processes (AOPs) are currently employed for this purpose, including photochemical degradation processes, photocatalysis, and chemical oxidation processes. However, despite encouraging laboratory scale data and some industrial scale tests, chemical oxidation detoxification is still restricted to a few experimental plants (Chiron et al., 2000).

An important drawback of these AOPs is that their operational costs are relatively high compared to those of biological treatments, which are, at present, the cheapest and the most compatible with the environment. However, the use of AOP as a pretreatment step to enhance the biodegradability of wastewater containing recalcitrant or inhibitory compounds can be justified if the resulting intermediates are easily degradable in a further biological treatment (Sarria et al., 2002).

Advanced oxidation processes although making use of different reacting systems, are all characterized by the same chemical feature: production of

hydroxyl radicals (HO·). Hydroxyl radicals are extraordinarily reactive species (oxidation potential 2.8 V), they attack the most part of organic molecules with rate constants usually in the order of 10^6 –10^9 $M^{-1}s^{-1}$ (Andreozzi et al., 1999). They are also characterized by a little selectivity of attack which is a useful attribute for an oxidant used in wastewater treatment and for solving pollution problems. The versatility of AOPs is also enhanced by the fact that they offer different possible ways for hydroxyl radicals production, thus allowing a better compliance with the specific treatment requirements (Malato et al., 2002).

Photochemical degradation processes

- UV/O_3
- UV/H_2O_2

Photocatalysis

- TiO_2/UV

Chemical oxidation processes

- O_3/H_2O_2
- H_2O_2/Fe^{2+}

Figure 1.1 List of advanced oxidation processes (AOPs)

1.2 Photocatalysis using UV/ TiO_2

Due to the worldwide application of intensive agricultural methods during the last few decades and to the large-scale development of the agrochemical industry, the variety and quantities of agrochemicals present in continental and marine natural waters has dramatically increased. Most pesticides are resistant to chemical and/or photochemical degradation under typical environmental

conditions (Grover and Cessna, 1991). There are high potential in the applications of AOPs for remediation of contaminated waters (Burrows et al., 2002). Photocatalysis using UV and titanium dioxide (TiO_2), a semiconductor, is one of the AOPs that may become an emerging technology in such area (Konstantinou and Albanis, 2002).

Photocatalytic reaction has been shown to be useful in destructing a wide range of air and/or water originated contaminants (Ollis, 1985; Ollis et al., 1991; Blount et al., 2001). Table 1.1 listed out the results of selected research (Peñuela and Barceló, 1998) on photocatalysis of some of the compounds. Titanium dioxide is broadly used as a photocatalyst because it is photochemically stable, non-toxic and cost little (Augugliaro et al., 1995; Topalov et al., 2000). One of the examples using titanium-dioxide induced photocatalytic reactions in aqueous systems is the mineralization of halogenated organic compounds, in which they are converted to carbon dioxide, water, and halide ions (Alfano et al., 1997). Photocatalytic degradation using UV/TiO_2 appears to be an effective strategy for degrading and mineralizing chlorinated pesticides (Bianco-Prevot et al., 1999, 2001; Doong et al., 2000).

Table 1.1 Results of selected research on photocatalysis of some of the compounds

Compound	Conditions		Results
	Chemical	Light Source	
Alachlor	TiO_2-H_2O_2	Xenon lamp	$t_{1/2}$ =17.3 min
Alachlor	TiO_2	240 nm	100 % removal: < 20 min
Chlorpyrifos	TiO_2-H_2O_2	Xenon lamp	$t_{1/2}$ =19.2 min
Endosulfan	TiO_2-H_2O_2	Xenon lamp	$t_{1/2}$ = 97 min
Bentazone	TiO_2 , pH 2	Xenon lamp	$t_{1/2}$ = 30 min
Bentazone	TiO_2 , pH 7	Xenon lamp	$t_{1/2}$ = 4 min
Fenitrothion	TiO_2	>340 nm	100 % mineralization: 50 min
Permethrin	TiO_2	sunlight	90 % conversion: 8 hr
Pentachlorophenol	TiO_2	Xenon lamp	Complete dechlorination: 3 hr
Lindane	TiO_2	>290 nm	100 % removal: 60 min
PCBs (aqueous solution)	TiO_2	Sunlight	80 % removal: 4 hr
PCBs (sediment)	TiO_2	Sunlight	50 % removal: 6 hr
Acid orange 7	TiO_2	Xenon lamp	80 % removal: 1 hr
Atrazine	TiO_2, Peroxydisulfate	Sunlight	98 % removal: 2 hr
Atrazine	TiO_2	Xenon lamp	100 % removal: 10 min
Trichloroethylene	TiO_2 on silica	Sunlight	95 % removal: < 3 min
Carbaryl	TiO_2	254 nm	$t_{1/2}$ = 26 s
Pendimethalin	TiO_2	240 nm	60 % removal: < 200 min
Malathion	TiO_2, H_2O_2	> 350 nm	$t_{1/2}$ = 100 min
1,2-Dichloroethylene	TiO_2, H_2O_2	Mercury lamp	100 % removal: < 1 hr

1.3 Reaction mechanism of photocatalysis using UV/ TiO_2

In general, photoinduced electrons (e^-) and positive holes (h^+) (see Eq. 1) are produced from TiO_2 under irradiation of UV light ($\lambda < 380$ nm), which has an energy greater than the band gap (3.2 eV) of TiO_2. These charged species can further generate free radicals under appropriate conditions, as shown in Eqs. 2 and 3 (San et al., 2002). The highly oxidizing positive hole has been considered to be the dominant oxidizing species contributing to the mineralization process resulting from the TiO_2 photocatalyst. Since the hole concentration is expected to be highest at the TiO_2 particles surface, many researchers such as Bekbölet et al. (1996), Sánchez et al. (1997) and Xu and Langford (2000) have reported that the degradation reaction is related to the adsorbed target compound onto the TiO_2 particles surface.

$$TiO_2 + h\nu \rightarrow TiO_2(e^- + h^+) \quad (1)$$

$$h^+ + OH^- \rightarrow OH\cdot \quad (2)$$

$$e^- + O_2 \rightarrow \cdot O_2^- \quad (3)$$

$$e^- + h^+ \rightarrow \text{thermal energy} \quad (4)$$

1.4 Review of past photocatalysis research

Adsorption of substrates onto the surface of TiO_2 where photons are adsorbed is a desirable feature to achieve maximal oxidation efficiency. TiO_2 has a polar surface and is not, itself, a good adsorbent for nonpolar organic molecules. On the other hand, the point of zero charge for TiO_2 is around pH 6 (Bianco-Prevot et al., 1999; Yang et al., 2001); below and above this pH value the surface of

TiO_2 particles is positively and negatively charged, respectively (see Figure 1.2). In many cases, electrostatic repulsion between this surface and the substrate occurs. Strategies devised to increase the adsorption of organic substrates on the catalyst surface have been centered on the use of TiO_2 (Ranjit et al., 2001; Aceituno et al., 2002).

In UV/TiO_2 process, the recombination of holes (h+) and electrons (e-) (see Eq. 4) has been regarded as the unfavorable or limiting process in photocatalysis using titanium dioxide suspensions. Over the past ten years, research has focused on reducing the effect of recombination of charges or enhancing photocatalysis performance by applying different techniques including the electrochemical method (Yu et al., 1997), surface modification of TiO_2 (Makarova et al., 2000), and adding an external electron acceptor such as hydrogen peroxide (H_2O_2) (Ollis et al., 1991).

A review of past research revealed that broadband light sources such as xenon lamp were used for studying photolysis or photocatalysis (Moza et al., 1992; Chiron et al., 1995; Peñuela and Barceló, 1996) or H_2O_2-assisted photocatalysis (Augugliaro et al., 1990; Dillert et al., 1996; Chen et al., 1998; Doong and Chang, 1998; Peñuela and Barceló, 1998, 2000; Cornish et al., 2000;, Dionysiou et al., 2000), whereas the use of different monochromatic UV wavelengths were seldom attempted, and may be interesting for such applications.

Photocatalysis reactions with the addition of hydrogen peroxide, which has been reported to exhibit appreciable rate increases when it is added to a photocatalysis process (Ollis et al., 1991; Aceituno et al., 2002); however, negative effects have also been reported on the use of H_2O_2 on the photocatalytic degradation of dichlorvos, trinitrotoluene and trinitrobenzene (Lu et al., 1994; Dillert et al., 1996). While many researchers reported the positive effect of H_2O_2 in the H_2O_2-assisted photocatalysis process, rate retardation has also often been reported without identifying the reasons. This contradiction is clarified in this study due to the different roles of H_2O_2 in the process at different UV wavelengths.

In addition to the performance of the treatment process, the study of the formation of by-products is also important. The information of formation and decomposition of the degradation intermediates or by-products are critical before a clean technology can be established. Chiron et al. (1997) have reviewed the use of AOPs for pesticide degradation and pointed out that information regarding the intermediates structures and reaction pathways are essential for the breakthrough of AOPs for pesticide elimination. The formation of toxic by-products during photocatalysis (Manilal et al., 1992; Minero, et al., 1995; Lu and Chen, 1997; Jardim et al., 1997; Chiron et al., 2000) and photosensitized degradation (Peñuela and Barceló, 1998) of chlorinated pesticides or organic compounds were often reported. Cost-effective treatment to complete compound mineralization is usually not feasible and the generation of by-products appears to be unavoidable with photocatalytic degradation. Identification of those by-products is the key to maximizing overall process efficiency (Malato et al., 2002).

Since the information of the reaction mechanism of photocatalysis of alachlor is very limited, and only a few intermediates were identified due to the limitations of conventional GC-MS (Moza et al., 1992; Peñuela and Barceló, 1996), the identifications of reaction intermediates in this study were performed by using the most recent technique: liquid chromatography mass spectrometry (LCMS) and MS/MS, which enables the determination of various soluble intermediates and reveals the degradation mechanisms and reaction pathways of the process in a more detailed scheme.

Two herbicides, alachlor and dicamba were studied in this research. Alachlor (2-chloro-2', 6'-diethyl-N-(methoxymethyl) acetanilide, see Figure 1.3 (a)) is a widely-used herbicide; it has been detected in ground water and rivers in the United States (Potter and Carpenter, 1995; Battaglin et al., 2000) and about 26 million pounds were used for agricultural purposes from 1990 to 1993 in the United States. The maximum contaminant level of alachlor for drinking water established by the USEPA is 2 μg/L (Larson %t al., 1999). Dicamba (2-methoxy-3,6-dichlorobenzoic acid, see Figure 1.3 (b)) is used as a post-emergence herbicide for the selective control of weeds of the buckwheat family in cereals. This chlorinated herbicide is also applied for the control of broadleaved weeds in pastures and rangeland grasses (Smith, 1974). Dicamba has been listed for restricted use due to its high potential for leaching in soils and for its persistence in ground water (Zhao et al., 1996) and potential for widespread contamination of ecosystems (Pavel et al., 1999). Since alachlor is neutral in nature and

dicamba is an acid, it is interesting to compare the their degradation performance in heterogeneous photocatalytic processes.

$TiO_2[H_2O]$ at pH = point of zero charge

$TiO_2[H_3O^+]$ at pH < point of zero charge

$TiO_2[OH^-]$ at pH > point of zero charge

Figure 1.2 Variation of surface charge of titanium dioxide

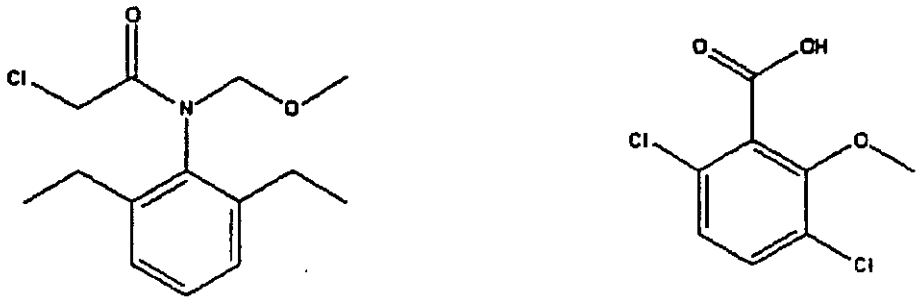

(a) (b)

Figure 1.3 The structure of (a) alachlor (2-chloro-2',6'-diethyl-N-(methoxymethyl) acetanilide, CAS no. 15972-60-8; molar mass = 269.7 g) and (b) dicamba (2-methoxy-3,6-dichlorobenzoic acid, CAS no. 1918-00-9; molar mass = 221 g)

1.5 Objectives

The objectives of this research are as follows:

1. To study the kinetic and performance of direct photolysis and photocatalytic degradations of alachlor and dicamba using three different monochromatic UV lamps (254 nm, 300 nm and 350 nm).
2. To compare and analyze the direct photolysis and photocatalysis quantum yields obtained at the three different monochromatic UV wavelengths.
3. To study the photocatalytic reactions of alachlor and dicamba under various conditions including the examination of the effects of different TiO_2 sources, TiO_2 dosages, initial pH and proton sources (HCl, H_3PO_4, HNO_3 and H_2SO_4).
4. To investigate and compare the effect of initial pH on the TOC decay with herbicide decay in photocatalysis reactions of alachlor and dicamba.
5. To study the influence of the addition of hydrogen peroxide (H_2O_2) in photocatalysis of alachlor and dicamba at the two different monochromatic near UV wavelengths (UV at 300 and 350 nm) with different H_2O_2 dosages.
6. To further evaluate the H_2O_2-assisted photocatalysis reactions of alachlor and dicamba at different initial pH.
7. To investigate the degradation mechanisms of alachlor in both the photocatalysis and H_2O_2-assisted photocatalysis reaction through intermediates identification using liquid chromatography-electrospray ionization-mass spectrometry (LC-ESI-MS) and MS/MS. TOC changes are also monitored simultaneously, so that the relationship between mineralization and alachlor degradation can be realized.

Chapter 2: Methodology

2.1 Chemicals

Alachlor $C_{14}H_{20}ClNO_2$ (99.7 % HPLC grade) and dicamba $C_8H_6Cl_2O_3$ (99 % HPLC grade) was purchased from Riedel-de Haën and Supleco respectively. Solubility of alachlor and dicamba are 240 mg/L and 8310 mg/L respectively. The initial concentration of alachlor and dicamba in all experiments was 22 μM. Two types of titanium dioxide, Anatase TiO_2-BDH (particle size of 40-500 μm, BET surface areas of 10.5 m^2/g (Palmisano et al., 1993)) and TiO_2-P25 (particle size of 30 nm, containing 70% Anatase and 30 % Rutile, BET surface areas of 50 m^2/g (Nargiello and Herz, 1993; Bekbölet and Balcioglu, 1996)) were used in this study for comparison, and were obtained from BDH and Degussa Corp. Japan, respectively. As the initial alachlor concentration was relative low in this study, it was necessary to use a lower TiO_2 dosage such that the degradation of alachlor could be monitored more accurately. The concentration of titanium dioxide used in most experiments was 5 mg/L unless otherwise stated. Acetonitrile of HPLC grade from LAB-SCAN was used in the preparation of the mobile phase in HPLC analysis without further purification. As alachlor has very low molar absorptivity at UV wavelengths above 280 nm, and low water solubility (240 mg/L), methanol (A.R. grade from LAB-SCAN) was used as the solvent to prepare a higher concentration of alachlor, so that the molar absorptivity and quantum yields of alachlor at 300 nm and 350 nm could be determined. All solutions were prepared using distilled-deionized water (resistivity 18 MΩ-cm) by a Barnsted NANO pure ultra-pure water system. After adding the target compound, TiO_2 and distilled-deionized water, diluted

inorganic acids/base (A. R. grade) including hydrochloric acid, sulphuric acid, phosphoric acid, nitric acid, and sodium hydroxide were used to adjust the initial pH of solutions to the pre-determined levels.

2.2 Methods

2.2.1 Experimental setup

All direct photolysis and photocatalysis experiments were conducted using an RPR-200 Rayonet photochemical reactor purchased from the South New England Ultraviolet Company. In each experiment, a quartz vessel (52 mm I.D × 470 mm length) filled with 500 mL sample solutions was placed inside the reactor and illuminated with monochromatic UV lamps (see Figure 2.1). A magnetic stirrer was located at the reactor's base such that a homogenous TiO_2 suspension could be maintained in the quartz vessel throughout the reaction; a cooling fan was also installed at the reactor base such that the experimental temperature maintained at 24 to 25 °C. In each experiment, at most sixteen phosphor-coated low-pressure mercury lamps were installed in the reactor. However, two 254 nm UV lamps, ten 300 nm "sunlight" UV lamps or ten 350 nm "blacklight" UV lamps were used in this study, so that the rate constants and quantum yield resulted form different wavelengths are comparable. The light intensity of 254 nm UV lamps was previously determined by a chemical actinometer, potassium ferrioxalate (Chu and Jafvert, 1994); since no significant difference was found between the measurement and the manufacturer's data, the intensities of the 300 and 350 nm UV lamps are therefore directly cited from the manufacturer's specifications, as illustrated in Table 3.1.

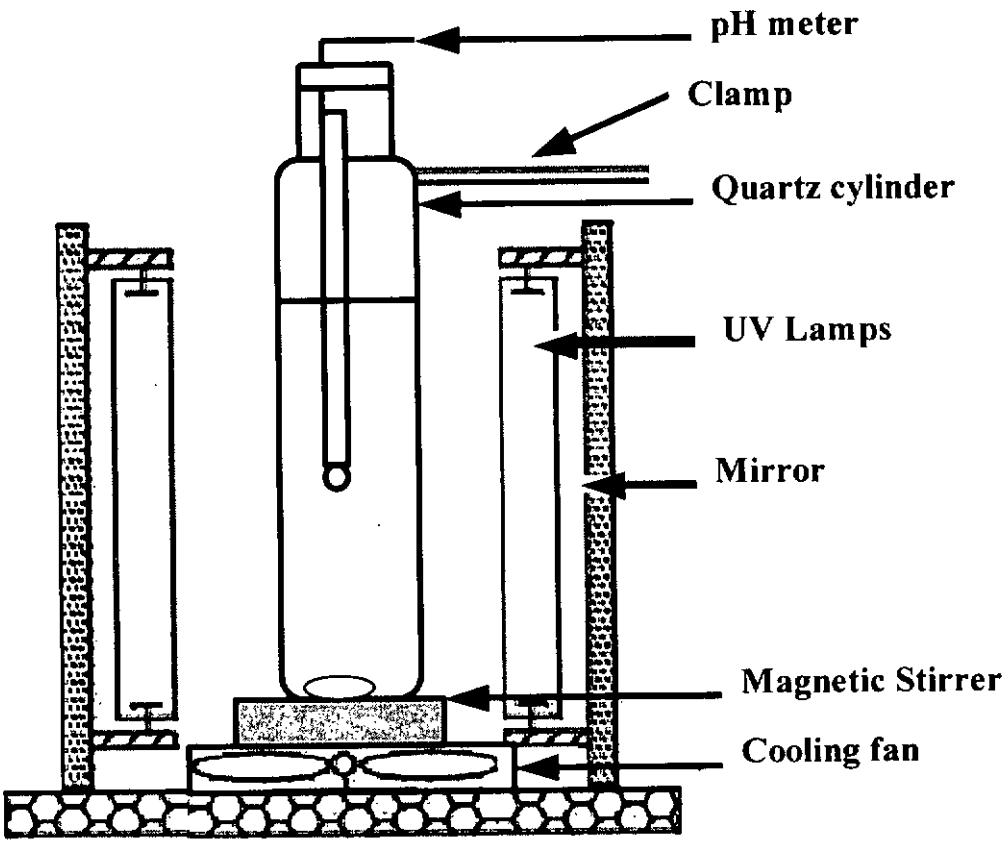

Figure 2.1 Experimental setup

2.2.2 HPLC and TOC analysis

Right after the addition of H_2O_2 (if any) to the reactor, the UV lamps were turned on to initiate the reaction. Samples were taken from the quartz vessel at different reaction times until the total degradation of the alachlor achieved 80% or higher. The collected samples were first centrifuged at 3000 rpm for 10 min using a Hettich ZENTRIFUGEN centrifuge to remove the titanium dioxide prior to chemical quantification. The remaining alachlor was then quantified by high performance liquid chromatography (HPLC). Two HPLC systems were used. The first HPLC system comprised a pump with a 100 μL injector, a Water™ SYMMETRY 5 μm C_{18} (3.9 x 150 mm) column, and a Water™ 486 UV/VIS Tunable Absorbance detector. The mobile phase of alachlor in this HPLC

consisted of 60% acetonitrile and 40% distilled-deionized water delivered at a flow rate of 1.0 ml/min. The second HPLC system comprised a Spectra SYSTEM® P4000 Gradient pump, a Spectra SYSTEM® AS3000 Autosampler with a 20μL injection loop, a ThermoQuest Hypersil® ODS (3μm 150 x 2.1 mm) column (for alachlor) or a 5 μm 4.6 mm ID x 250 mm PinnacleTM octyl amine column (Restek) (for dicamba) and a SpectraSYSTEM® uv6000LP photodiode array UV detector. A Spectronic Genesys^{TM} 5 UV/VIS spectrophotometer was used to obtain the UV spectrum of alachlor, dicamba and hydrogen peroxide. The maximum absorption wavelength (λ_{max}) selected to detect alachlor and dicamba was 265 and 203 nm, respectively. The mobile phase for alachlor in the second HPLC system consisted of 70% acetonitrile and 30% distilled-deionized water, and was delivered at a flow rate of 0.2 ml/min, whereas the mobile phase for dicamba consisted of 20 % acetonitrile and 80 % distilled-deionized water, and was delivered at a flow rate of 1 ml/min. The mobile phase was used to flush column for at least 1 hour to obtain a stable pressure before starting each experiment. TOC changes were also monitored simultaneously, so that the relationship between mineralization and herbicide degradation could be realized. The TOC decay was determined using a SHIMADZU TOC 5000A equipped with an ASI-5000A autosampler. For both HPLC and TOC analysis, a 4-points standard curve was plotted before starting each experiment.

2.2.3 MS analysis

The study of intermediates in the alachlor photocatalysis was performed using a Finnigan LCQ™ DUO ion trap mass spectrometer by electrospray ionization (ESI), which was coupled to the LC. As suggested by other

researchers (Thurman et al., 2001; Zang et al., 2002), it was operated in positive ionization mode. To minimize unwanted metal adducts formation and increase the detection sensitivity/ionization performance, the entering of LC eluent into the MS detector was set to be delayed by 0.5 min in order to remove the salts. Nitrogen generated by the NITROX nitrogen generator was used as both a sheath and auxiliary gas. The capillary temperature was 200°C and the rates of flow of sheath and auxiliary gas into the atmospheric pressure ionization region were 0.6 and 0.0 L/min, respectively. The damping gas in the mass analyzer was helium, which was purchased from Hong Kong Special Gas Co. Ltd. Helium also acted as the collision gas during the collision-induced dissociation (CID) process in the MS/MS analysis. By direct infusion of alachlor into the mass spectrometer, the ion optics setting was optimized using the LCQ Tune plus software. MS data were compared against the blank and standard. Before and after each experiment, A.R. grade methanol was used to clean the capillary, needle spray and spray cone.

Chapter 3: Results and Discussion

3.1 Direct photolysis and photocatalysis with different sources of TiO_2

The photodecay of alachlor by UV with and without the presence of TiO_2 was investigated by using two different types of commercial titanium dioxide, TiO_2-BDH and TiO_2-P25. Both the direct photolysis and photocatalysis of alachlor and dicamba were found to follow pseudo first-order decay kinetics at 300 nm UV illumination, as shown in Figure 3.1. The rate constants in these three processes were in the order of 0.012, 0.038, and 0.128 min^{-1} for alachlor and 0.028, 0.039, and 0.082 min^{-1} for dicamba in direct photolysis, photocatalysis with TiO_2-BDH, and photocatalysis with TiO_2-P25 respectively. The lower rate of direct photolysis at UV 300 nm was due to the practically low absorption of the two probes at 300 nm. The measured molar absorptivity (ε_λ) of alachlor and dicamba at 300 nm was 3.0 and 2.9 cm^{-1} M^{-1} respectively. Besides, 300 nm is a relative low-energy radiation compared to that of 254 nm, which is the wavelength normally used for disinfection and photodegradation purposes (Chu, 1999).

The photocatalysis of alachlor using TiO_2-BDH or TiO_2-P25 can improve the decay rate by 3 and 11 times respectively compared to that of direct photolysis, and the photocatalysis of dicamba using TiO_2-BDH or TiO_2-P25 can improve the decay rate by 1.4 and 3 times respectively compared to that of direct photolysis. Apparently, the significant improvement in alachlor or dicamba decay is mainly contributed by the presence of a parallel (or additional) pathway of photocatalysis that co-exists with the direct photolysis. However, it is interesting

to learn that the use of different types of TiO_2 may result in significant differences in the overall performance, which is likely attributed to the different physiochemical properties of TiO_2. Upon the UV illumination of the TiO_2 particles, electrons and positive holes are generated simultaneously. Theoretically, the electrons are free to diffuse into the aqueous phase, therefore the positively charged holes are likely accumulated on the TiO_2 surface in order to maintain a proper charge balance. Under these circumstances, the hydroxyl radical concentration is expected to be highest at the TiO_2 particles surface, which makes the UV-induced photocatalysis a surface-dependent process. As TiO_2-P25 has a much larger unit surface area and a much smaller average particle size (see Methodology (Chemicals) section) than TiO_2-BDH, this justifies the higher TiO_2-P25 performance over TiO_2-BDH. TiO_2-P25 was therefore used as the exclusive TiO_2 source for the rest of the study.

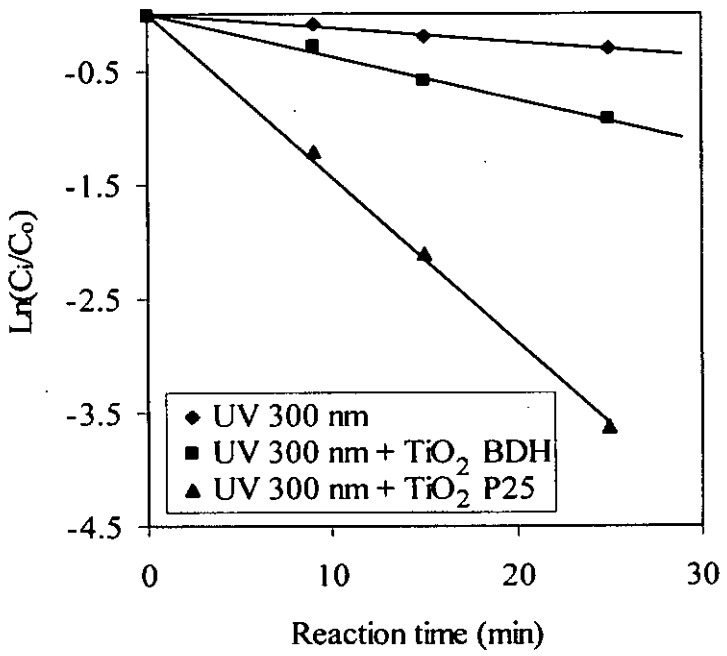

(a)

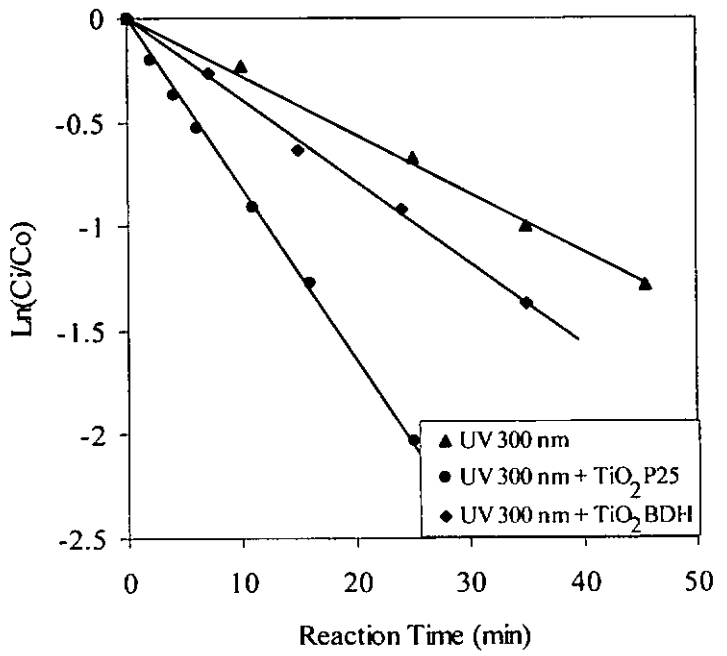

(b)

Figure 3.1 The pseudo first-order decay of (a) alachlor and (b) dicamba via direct photolysis and photocatalysis (with TiO_2-BDH or TiO_2-P25) illuminated at 300 nm, where the TiO_2 dosage is 5 mg/L and the initial pH is 6.

3.2 Comparison of the quantum yields for both direct photolysis and photocatalysis

Since the photodecay of alachlor or dicamba involves both direct photolysis and photocatalysis, and the degree of participation of both pathways may be varied if different UV sources (wavelengths) are applied, it is necessary to investigate the alachlor or dicamba decay by both direct photolysis and photocatalysis at different UV wavelengths. The study was conducted by quantum yield examination, so that the differences of light intensities among different light sources could be eliminated and the results become comparable. Quantum yields of first-order alachlor or dicamba photodecay with monochromatic light sources for both the direct photolysis and photocatalysis could be calculated using the following equation (Chu and Jafvert, 1994; Chu et al. 1998):

$$\phi = \frac{k}{2.303 I_\lambda \varepsilon_\lambda \lambda} \qquad (5)$$

where k (min^{-1}) is the pseudo first-order rate constant, ϕ is the quantum yield, I_λ (Einstein L^{-1} min^{-1}) is the incident light intensity at wavelength λ, ε_λ (cm^{-1} M^{-1}) is the molar absorptivity at wavelength λ, and l is the cell path length (cm). The results of alachlor or dicamba decay quantum yields through either direct photolysis or photocatalysis under the illumination of UV at 254 nm, 300 nm and 350 nm are summarized in Table 3.1.

The quantum yields of direct photolysis were found to increase with the molar absorption coefficient and decrease with the increase of UV wavelength, in which the direct photolysis of alachlor and dicamba at 254 nm gives the highest

quantum yield (0.095 for alachlor, 0.140 for dicamba), and followed by 300 nm (0.051 for alachlor, 0.121 for dicamba) and 350 mm (0.008 for alachlor, 0.058 for dicamba). This observation can be rationalized by two mechanisms. First, as the molar absorptivity of the target compound at a particular wavelength is high, a higher fraction of the compound will be involved in the direct photolysis process within a fixed time interval, resulting in higher decay rates (*i.e.* a higher k in Eq. 5). Secondly, the lower the UV wavelength, the higher the radiation energy, which facilitates the destruction of the target compound through direct photolysis. However, in the presence of TiO_2, the photocatalysis quantum yields obtained with different monochromatic UV light show a different descending order of 300 nm (0.537 for alachlor, 0.354 for dicamba), 350 nm (0.208 for alachlor, 0.289 for dicamba), and 254 nm (0.121 for alachlor, 0.174 for dicamba). Photocatalysis of alachlor using UV 300 nm achieves the highest quantum yield, which is about 6, 11, and 67 times over the direct photolysis quantum yields at 254, 300, and 350 nm, respectively. Similarly, Photocatalysis quantum yield of dicamba using 300 nm is about 2.5, 3.0, and 6.0 times over the direct photolysis quantum yields at 254, 300, and 350 nm, respectively.

Although the direct photolysis rate is the highest at UV 254 nm, there is little difference between the direct photolysis quantum yield (0.095 for alachlor, 0.140 for dicamba), and the photocatalysis quantum yield (0.121 for alachlor, 0.174 for dicamba), suggesting that the photodecay of alachlor or dicamba at UV 254 nm was dominated by direct photolysis even if the TiO_2 was present. In other words, the use of TiO_2-induced photocatalysis at UV 254 nm is not an effective process for alachlor or dicamba decay. The use of TiO_2 at UV 350 and 300 nm, however,

gives a significant increment in photocatalysis quantum yields: 26 times greater for alachlor at 350 nm (5 for dicamba), and 11 times greater for alachlor at 300 nm (3 for dicamba) than their corresponding direct photolysis quantum yields, indicating that the application of a TiO_2 mediated photocatalytic reaction is effective under near UV ranges. Since 300 nm is among the best for alachlor decay, it was used as the sole light source for the study of the effect of TiO_2 dosages, initial pH and proton sources.

Table 3.1 Comparison of direct photolysis and photocatalysis of alachlor and dicamba at different UV wavelengths (the dosage of TiO_2 -P25 is 5 mg/L, and the initial pH is 6)

UV wavelength, λ_i (nm)	254	300	350
Total Power consumption (W)	70	210	240
Photo-intensity, I (Einstein L^{-1} min^{-1})	1.80×10^{-4}	6.64×10^{-3}	3.24×10^{-2}
Molar absorptivity of alachlor, $\varepsilon_{\lambda i}$ (cm^{-1} M^{-1})	428.0	3.0	1.6
Molar absorptivity of dicamba, $\varepsilon_{\lambda i}$ (cm^{-1} M^{-1})	262	2.9	0.6
Photolysis rate constant of alachlor, k_{1a} (min^{-1})	0.088	0.012	0.005
Photolysis rate constant of dicamba, k_{2a} (min^{-1})	0.079	0.027	0.014
Direct photolysis quantum yield of alachlor, ϕ_{1a}	0.095	0.051	0.008
Direct photolysis quantum yield of dicamba, ϕ_{2b}	0.140	0.121	0.058
Photocatalysis rate constant of alachlor, k_{1b} (min^{-1})	0.112	0.128	0.129
Photocatalysis rate constant of dicamba, k_{2b} (min^{-1})	0.098	0.082	0.067
Photocatalysis quantum yield of alachlor, ϕ_{2a}	0.121	0.537	0.208
Photocatalysis quantum yield of dicamba, ϕ_{2b}	0.174	0.354	0.289

3.3 Effect of TiO_2 dosages

The effect of different dosages of TiO_2-P25 on the photocatalytic degradation rates of alachlor and dicamba were examined. Figure 3.2 shows the variation of pseudo first-order rate constants with five different TiO_2-P25 dosages at 5, 25, 50, 75 and 100 mg/L under UV illumination at 300 nm, in which the photocatalytic degradation rates of alachlor and dicamba were found to increase with TiO_2 dosages, but the reaction was retarded at higher TiO_2 dosages. The increase in the rates is likely due to the increase in the total surface area (or number of active sites) available for photocatalytic reaction as the dosage of TiO_2 increased. However, when TiO_2 was overdosed, the intensity of incident UV light was attenuated because of the decreased light penetration and increased light scattering, which embedded the positive effect coming from the dosage increment and therefore the overall performance reduced.

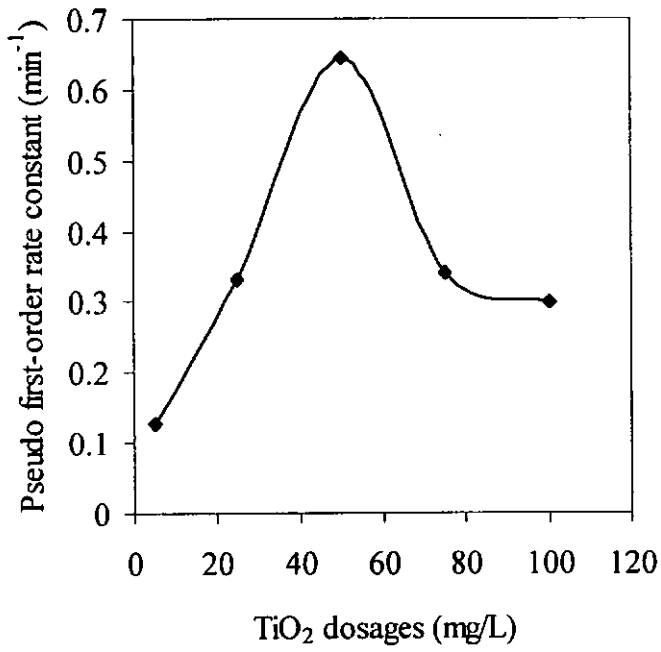

(a)

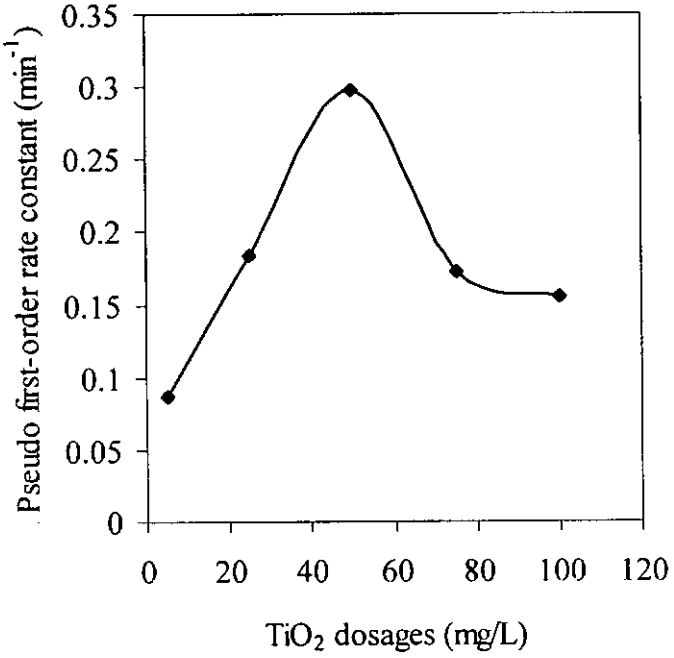

(b)

Figure 3.2 The pseudo first-order photodecay of (a) alachlor and (b) dicamba at various dosages of TiO_2-P25, where the initial pH level is 6.

3.4 Effects of initial pH

The effect of different initial pH levels on the photocatalytic degradation rates of alachlor was investigated. In general, the photocatalytic degradations rate was found to slightly depend on pH, as shown in Figure 3.3 (a). About 22 % increase in rate constant was observed as pH increased from pH 3.3 to pH 11.3. The rate increment is also likely due to the increase of hydroxyl ions in the solution, which was suggested to be critical in determining the concentration of hydroxyl radicals (HO·) in a UV photolysis process (Chu and Jafvert, 1994) or an oxidation process (Chu and Ma, 2000). At high initial pH, more hydroxide ions (OH^-) in the solution induced the generation of hydroxyl radicals, which came from the photooxidation of OH^- by holes forming on the titanium dioxide surface (see Eq. 2). Since hydroxyl free radical is the dominant oxidizing species in the photocatalytic process, the photodecay of alachlor is therefore accelerated in an alkaline medium. Similar reaction has been suggested by a number of researchers such as Ollis, et al. (1991), Sánchez, et al. (1997) and Bianco-Prevot, et al. (1999).

The effect of different initial pH levels on the photocatalytic degradation rates of dicamba was also investigated. The photocatalytic degradation rate was found to increase with initial pH from acidic to weak alkaline medium, as shown in Figure 3.3 (b). About 1.72 times rate enhancement was observed as pH increased from pH 3.3 to pH 8.5. However, further increment of pH would retard the rates, which could be explained by the effect of charges attraction or repulsion between TiO_2 particles and dicamba molecules or hydroxide ions (OH^-). The pK_a of dicamba is 1.93 (Zhao et al., 1996) and the point of zero charge of

TiO_2 particles is around pH 6. At acidic to neutral medium (i.e. low hydroxide ions concentration), the effect of charges attraction between negatively charged dicamba molecules and positively charged TiO_2 particles favor the coupling of dicamba molecules with TiO_2 particles. Since the density of the hydroxyl radicals is presumably highest near the surface of the TiO_2 particles and decreases rapidly with distance from the surface of TiO_2 particles, the favored coupling of the dicamba molecules with TiO_2 particles enhanced the dicamba degradation. However, when pH was increased above the point of zero charge of TiO_2 particles, the effect of charges repulsion between negatively charged dicamba molecules (or even hydroxide ions) and negatively charged TiO_2 particles became significant and eventually outweighed the positive effect resulting from the elevated hydroxide ion concentration.

TOC analysis was carried out along with the alachlor decay at three different initial pH levels of 3.1, 6.0 and 10.2, and the results are shown in Figure 3.4. At initial pH of 10.2, about 70 % of the TOC was removed (or mineralized) at reaction time of 130 min. In general, the decay of TOC could be divided into three stages: the first stage was the lag phase, where the TOC reduction was insignificant because the dominant reaction was the decay of alachlor to primary intermediates. These primary intermediates carry high molecular weights, and the benzene rings remain intact. The lag phase was followed by a mild TOC decay, in which about 80 % of the alachlor was decayed; the decay of high molecular weight intermediates (to lower ones) was initiated and became the dominant process. In the final stage, over 90% of alachlor was removed and the TOC decay rate increased significantly, indicating that the dominant decaying

species were small molecules. About 60 to 70 % of the TOC was removed (or mineralized) at 130 min. The different stages of TOC decay for alachlor can also be verified by the evolution profiles of different molecular weight intermediates and the relevant results will be illustrated later (section 3.8 and 3.9) in analyzing the alachlor degradation mechanism.

TOC decay was also investigated in parallel with the dicamba degradation at different initial pH levels (see Figure 3.5). The TOC decay for dicamba was comparatively faster than that of alachlor, and similarly, the decay of TOC for dicamba could be divided into two stages. The first stage was a short lag-phase, where the TOC reduction was slow because the mechanism of dicamba degradation was likely initiated by branch dissociations (e.g. dechlorination) and the benzene ring remained intact. The lag-phase was terminated after about 30 minutes, and followed by a faster pseudo first-order TOC decay, in which the mineralization of intermediates apparently became the dominant mechanism. In addition, similar to that of dicamba decay, the TOC decay was also accelerated at higher pH, 76 and 87% of the TOC was mineralized at pH 3.3 and 8.5, respectively after 110 min of reaction.

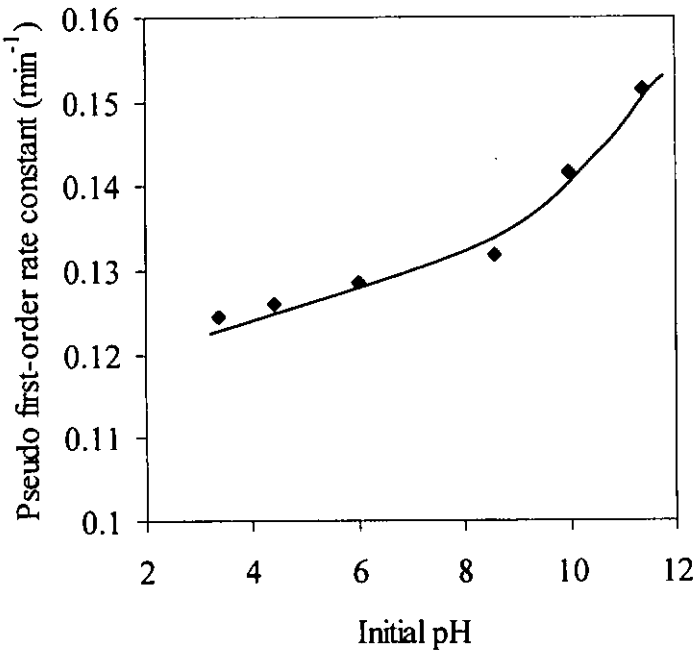

(a)

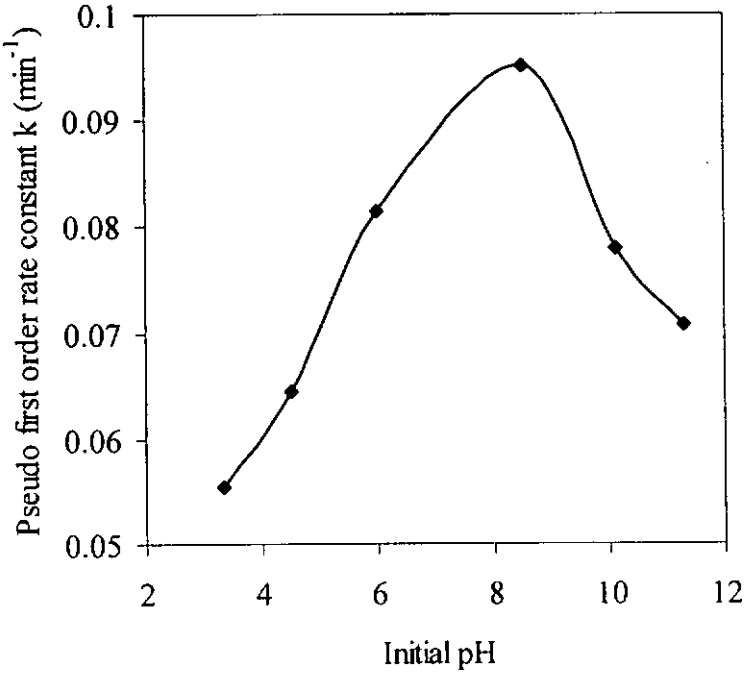

(b)

Figure 3.3 Variation of pseudo first-order rate constants with initial pH in photocatalysis of (a) alachlor and (b) dicamba under the illumination of UV 300 nm, with a TiO_2-P25 dosage of 5 mg/L.

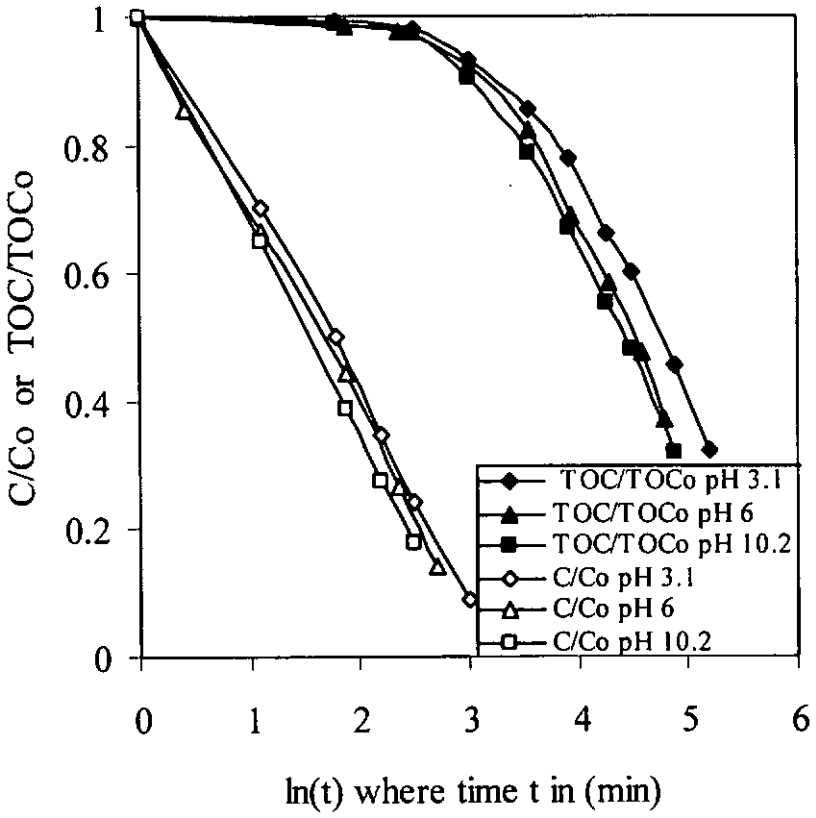

Figure 3.4 The photocatalytic decay of alachlor and TOC at initial pH levels of 3.1, 6.0 and 10.2.

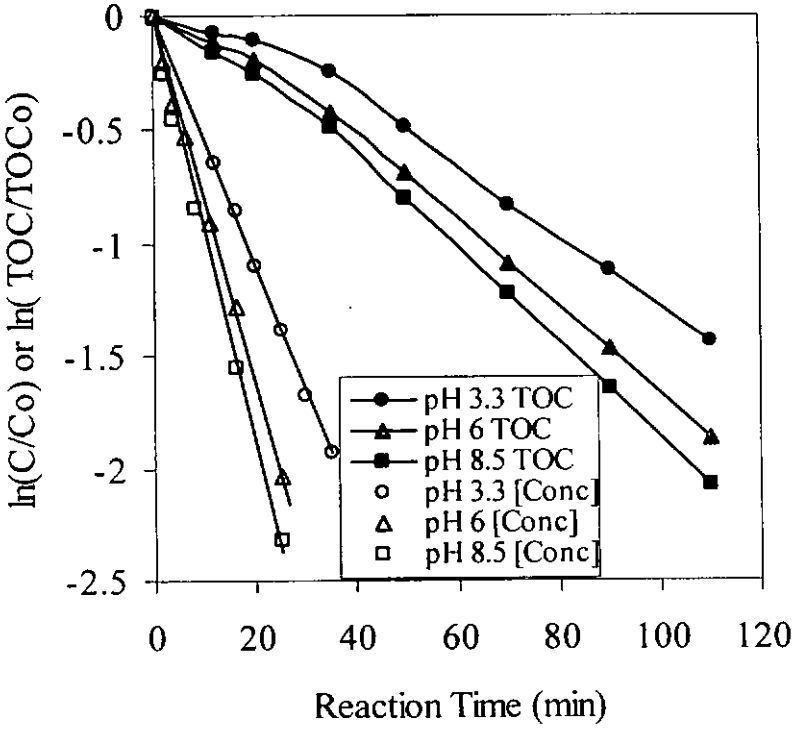

Figure 3.5 Comparison of the photocatalytic decay of dicamba and TOC at 300 nm of UV at initial pH levels of 3.3, 6 and 8.5.

3.5 Effects of proton sources

In addition, it is interesting to note that the different proton sources (*i.e.* the associated counter anions that come with protons) can alter the reaction of alachlor photocatalysis to different degrees. At first, the HCl was used as the exclusive source of protons in adjusting the pH levels in the study. However, if the proton source was replaced by other inorganic acids such as H_3PO_4, HNO_3, and H_2SO_4, significant retardation of the reaction rates was observed (see Figure 3.6 (a)). The photocatalytic degradation of alachlor no longer exactly follows pseudo first-order decay kinetics; instead, it can be divided into three stages. A lag stage (with a much slower decay rate) occurred initially in the reaction and was followed by a transition stage, in which the effect of the rate retardation was gradually reduced, then a much faster pseudo first-order decay reappeared in the final stage of the reaction. Similar results have been reported previously by Chen et al. (1997), suggesting that inorganic anions were capable of inhibiting the photocatalytic degradation of dichloroethane in an aqueous suspension of TiO_2.

Since alachlor is neutral in nature, the electrostatic attractions between alachlor molecules and TiO_2 particles can be ignored. The initial lag-stage is likely the result of the adsorption of anions on the surface of TiO_2 particles, and the isolation of the alachlor molecules from the reaction. As different proton sources were applied to the solution, different counter anions were involved in the reaction. As TiO_2 particles are positively charged at pH below its point of zero charge which is around pH 6, the presence of inorganic anions can be attracted by the positive charged TiO_2 particles and form a layer of charged

barriers around the TiO_2 particles, which hinders the collision between the alachlor molecule and the TiO_2 particles. Since the density of the hydroxyl radicals is presumably highest near the surface of the TiO_2 particles and decreases rapidly with distance from the surface of TiO_2 particles, the inhibition of the coupling of the alachlor molecule with titanium dioxide particles results in rate retardation. This assumption can be partly justified by the molecular size of the anions involved: judging from Figure 3.6 (a), the only anion that does not cause significant rate retardation is Cl^-, because its molecular weight is the smallest among the others (NO_3^-, SO_4^{2-}, and $H_2PO_4^-$). Moreover, another cause of the different extent of rate retardation may be the different binding ability of anions (acting as ligands) at the TiO_2 surface. Similar binding mechanism was also suggested by Chen et al. (1997) and Connor and McQuillan (1999)

Subsequent to the lag-stage, the reaction accelerates progressively. This is most likely due to the formation of intermediates, which may accumulate and form higher concentrations near the TiO_2 particles. Since the intermediates are similar to alachlor in nature (an organic compound), they have stronger affinity to alachlor molecules and may become a bridge or a good coupler to couple TiO_2 particles with un-reacted alachlor molecules, where the coupling mechanism is suggested to be important in promoting the TiO_2 related-photocatalytic reaction (Makarova et al. 2000). As the numbers of the couples increase, they compete with the active sites on the TiO_2 surface with anions and form more couples, such that the effect of anion inhibition is progressively reduced. As a result, the effect of rate retardation due to the presence of anions with large molecular size is reduced, and eventually the pseudo first-order decay kinetic is resumed again.

The different extent of rate retardation caused by the use of different proton sources was also found in photocatalysis of dicamba (see Figure 3.6 (b)) except that the lag phase was not observed. The result can be explained by considering the charge effects of alachlor and dicamba. The major difference between the two herbicides in the reaction was that there are attractions between the negatively charged dicamba molecules (an acid) and the positive charged TiO_2 particles, and this was not happened for alachlor. As a result, the condition of using reaction intermediates as couplers is not crucial for dicamba such that the lag phase for alachlor was not observed.

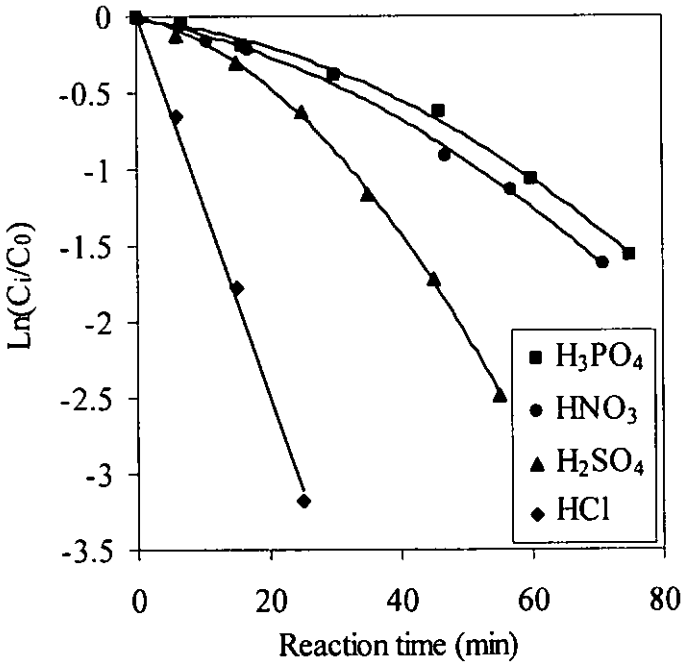

(a)

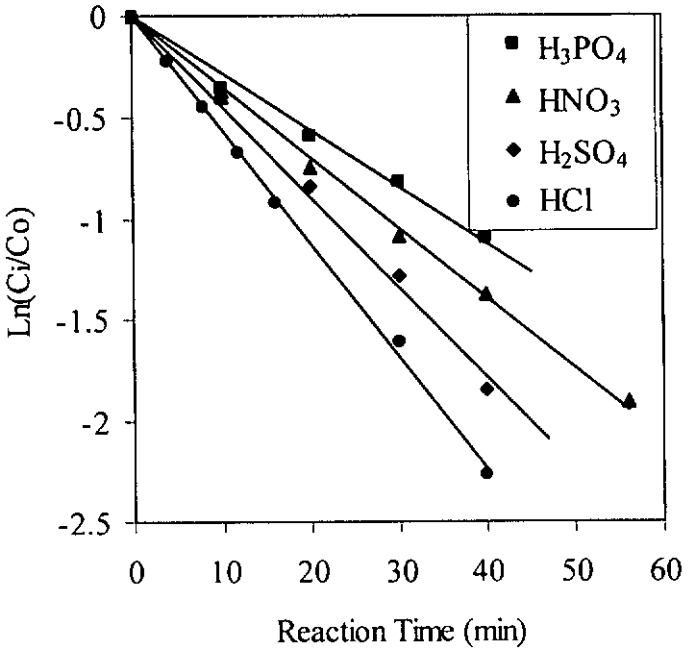

(b)

Figure 3.6 Effect of using different proton sources (HCL, H_2SO_4, H_3PO_4 and HNO_3) on the photocatalytic decay of (a) alachlor and (b) dicamba by 300 nm of UV, with a TiO_2-P25 dosage of 5 mg/L at an initial pH of 3.3.

3.6 Effect of H_2O_2 in improving and retarding the photocatalysis process

Since the photocatalysis rates of alachlor and dicamba at the two different wavelengths are about the same order, it is worthwhile comparing the possible further rate improvement of TiO_2 photocatalysis assisted by H_2O_2 at these wavelengths. To investigate the effect of adding H_2O_2 to the photocatalysis of dicamba, experiments with different dosages of H_2O_2 were carried out using two near UV wavelengths of 300 and 350 nm. At 300 nm of light illumination, eight different dosages of H_2O_2 (0.049, 0.25, 0.74, 1.24, 4.94, 9.88, 61.7 and 124.0 mmol/L) were applied to the reaction, and the results are shown in Figure 3.7 and Figure 3.8 at either low (a) or high (b) ranges of H_2O_2 dosages. The reaction rate was found to increase with H_2O_2 dosages at low H_2O_2 dosages. The optimal H_2O_2 dosage for both alachlor and dicamba is 4.94 mmol/L. At maximum, 3.3 and 2.4 times rate increments were achieved for alachlor and dicamba respectively at the optimal H_2O_2 dosage of 4.94 mmol/L compared to that of sole photocatalysis without H_2O_2. Above this optimal dosage, however, the overdose of H_2O_2 retards the photocatalytic rates. The rate improvement at lower H_2O_2 dosages is probably due to the following reasons. First, the direct photolysis of H_2O_2 by UV light can generate hydroxyl radicals (Chu and Choy, 2002), which are likely to be the dominant rate-improving mechanism in this process (Eq. 6). Another minor mechanism proposed by (Ollis et al., 1991) and (Ilisz et al., 1998) may partially contribute to the rate enhancement, in which H_2O_2 is suggested to be a better electron acceptor than oxygen. This would reduce the chances of electrons–holes recombination (*i.e.* the termination of excited components), an undesirable process in the photocatalytic process, which may generate one

hydroxyl radical as shown in Eq. 7 (Wei et al., 1990; Doong and Chang, 1998; Gao et al., 2002), rather than the weaker $\cdot O_2^-$ radical (as indicated in Eq. 3).

$$H_2O_2 + h\nu \rightarrow 2HO\cdot \quad (6)$$

$$e^- + H_2O_2 \rightarrow HO\cdot + OH^- \quad (7)$$

At high H_2O_2 dosage, however, the excess H_2O_2 molecules scavenge the valuable hydroxyl radicals that was generated by either the direct photolysis of H_2O_2 (Eq. 6) or the photooxidation of OH^- by h^+ (Eq. 2), and form a much weaker oxidant $HO_2\cdot$ (Eq. 8). Therefore, the total oxidation capabilities of the system are largely reduced (Eq. 9) and the rates retarded (Jenny and Pichat, 1991; Dionysiou et al., 2000).

$$H_2O_2 + HO\cdot \rightarrow H_2O + HO_2\cdot \quad (8)$$

$$HO_2\cdot + HO\cdot \rightarrow H_2O + O_2 \quad (9)$$

Similarly, different dosages of H_2O_2 were applied to the alachlor and dicamba photocatalysis process at UV 350 nm. It is interesting to note that no rate improvement was observed at all; instead, the higher the H_2O_2 dose, the lower the reaction rate; the comparison of the photocatalytic rates at the two wavelengths is summarized in Figure 3.9. At a very low H_2O_2 dosage of 0.0024 mmol/L, the rate constant was about the same as that of sole photocatalysis without H_2O_2. Any further addition of H_2O_2 could retard the reaction. This observation is likely attributed to the 50 times difference of molar absorptivity of H_2O_2 at 300 and 350 nm, which are 80 and 1.6 cm^{-1} L $mole^{-1}$, respectively. As

H_2O_2 has extremely low absorption at 350 nm, the critical direct photolysis of H_2O_2 generating hydroxyl radicals (Eq. 6) is insignificant, and hence free H_2O_2 is most likely to be present at relatively high levels (*i.e.* overdosed), which embedded other minor rate-improving mechanisms (*e.g.* Eq. 7), and a rate retardation was observed. The use of H_2O_2 in photocatalytic reaction at 300nm is therefore used exclusively for the rest of this study.

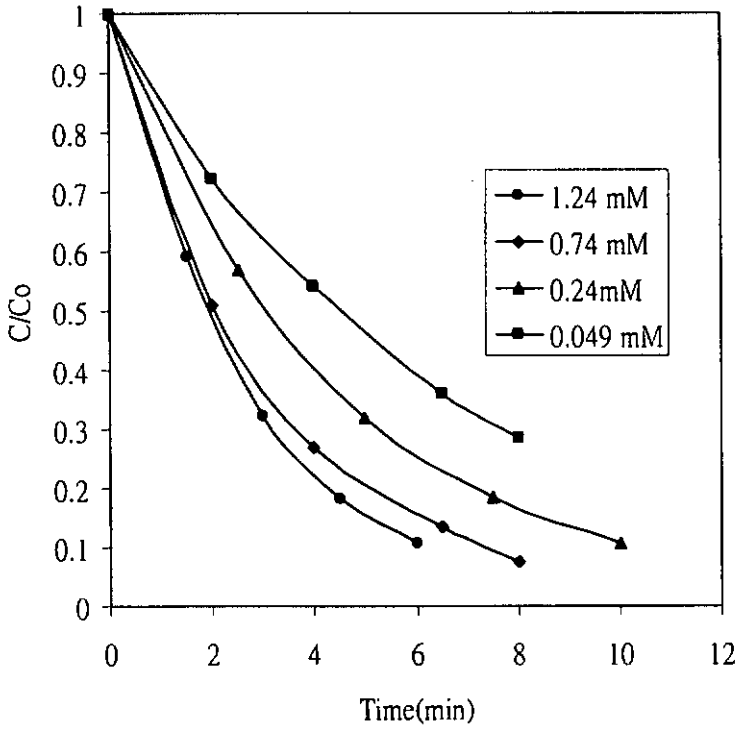

(a)

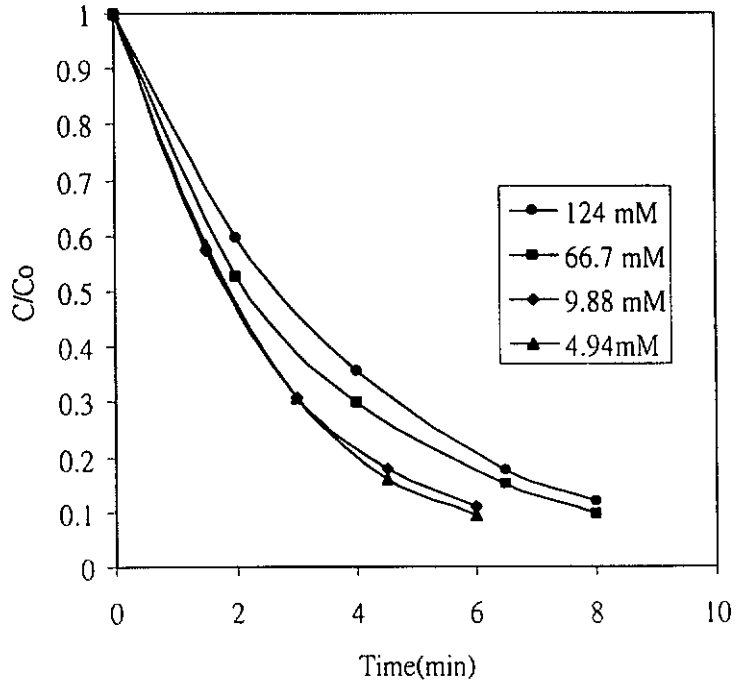

(b)

Figure 3.7 The photocatalytic decay of alachlor at (a) low (0.05 to 1.24 mmol/L) and (b) high (4.94 to 124.0 mmol/L) H_2O_2 dosages at 300 nm, where the [TiO_2] was 5 mg/L and the initial pH level was 6.

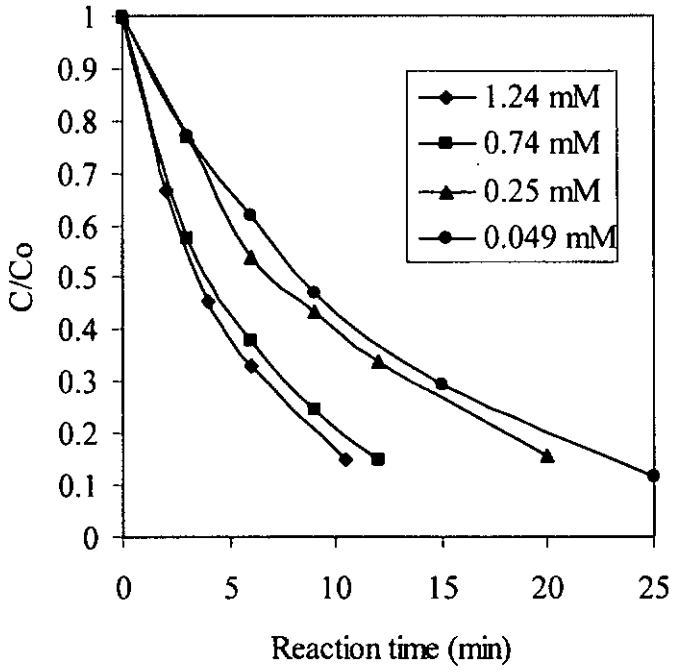

(a)

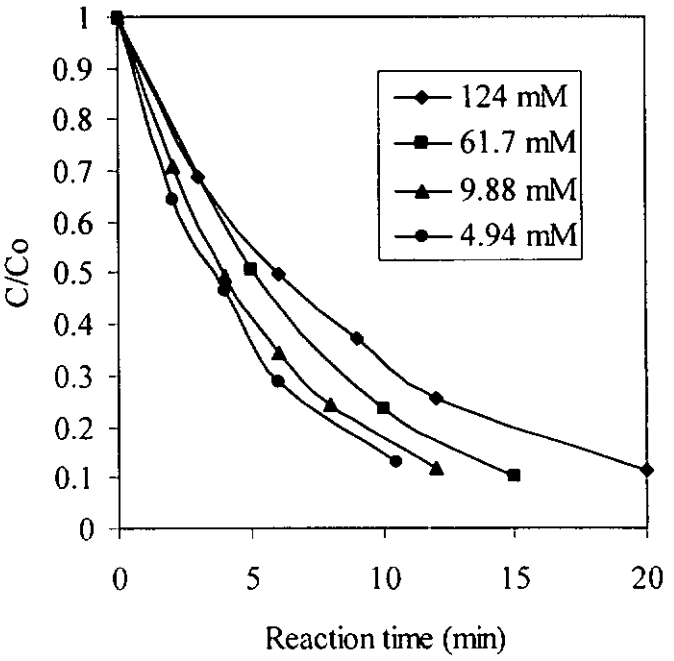

(b)

Figure 3.8 The photocatalytic decay of dicamba at (a) low (0.049 to 1.24 mmol/L) and (b) high (4.94 to 124 mmol/L) H_2O_2 dosages by 300 nm of UV at initial pH level of 6.

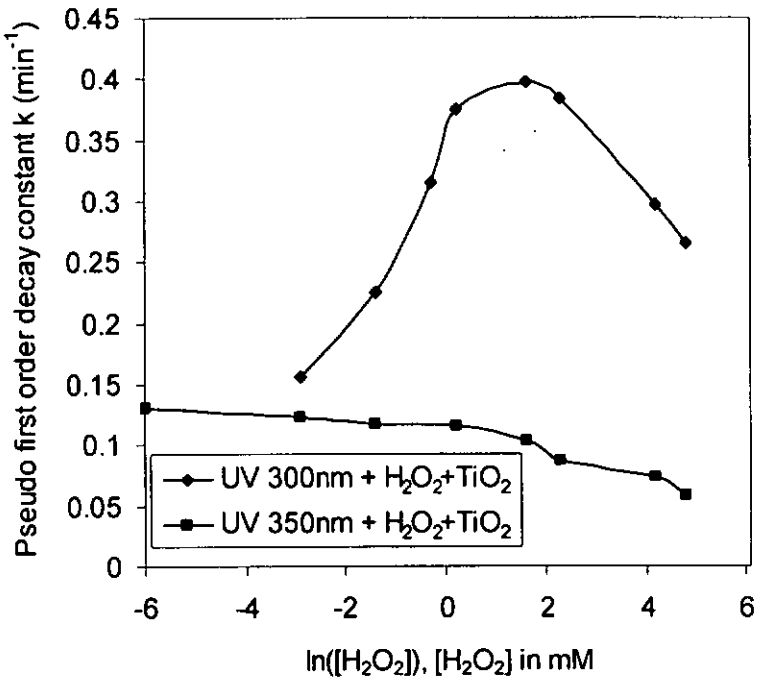

(a)

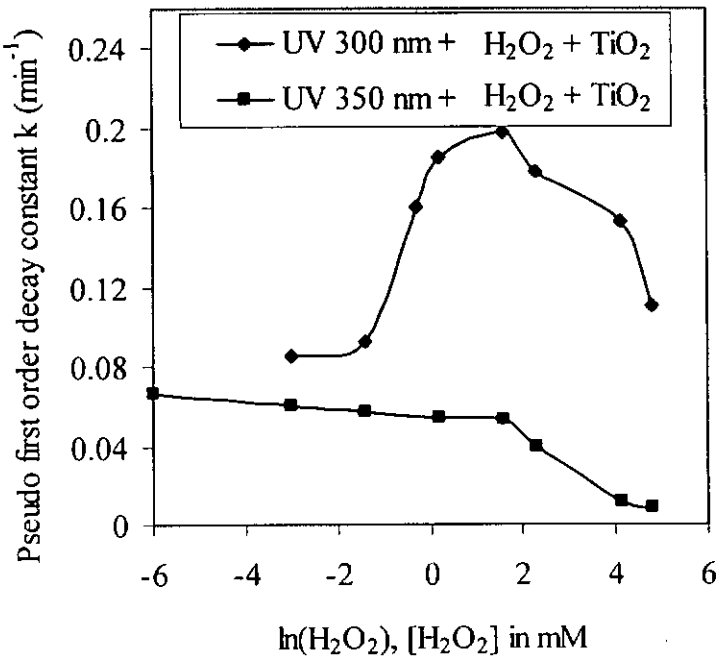

(b)

Figure 3.9 Variation of pseudo-first-order decay constant k (min^{-1}) of H_2O_2-assisted photocatalysis of (a) alachlor and (b) dicamba at various H_2O_2 dosages by either 300 or 350 nm at an initial pH level of 6.

3.7 Effect of initial pH on H_2O_2-assisted photocatalysis

The effect of initial pH on alachlor and dicamba photocatalysis with the addition of an optimal dosage of H_2O_2 was then studied as illustrated in Figure 3.10 and Figure 3.11. The variation of rate constants with initial pH for alachlor and dicamba in H_2O_2-assisted photocatalysis experiments are shown in Figure 3.12. In general, the reaction rates for both alachlor and dicamba gradually increased with increments of initial pH level, and an optimal pH was found at 6. The further elevation of the solution pH retarded the rates. The results were likely due to the fact that in an alkaline medium, H_2O_2 becomes unstable, and rapidly decays into water and oxygen, even in the presence of UV light (Chu, 2001). This assumption can be justified by the rate constant obtained for both alachlor and dicamba at about pH 11 in H_2O_2 assisted photocatalysis, which was smaller or about the same as that in photocatalysis experiment without the addition of H_2O_2. In addition, the CO_2 level in the solution keeps increasing during the reaction, either generated by the decay of herbicides or by the dissolution form the air; the former is justified by the TOC analysis and the latter confirmed by a blank test with a contribution up to 0.4 mg/L. Because the first and second pk_a of H_2CO_3 is 6.3 and 10.3, when the solution pH is higher than 6, the dominant specie of carbonate system will either be bicarbonate ions or carbonate ions. As both of them are radical scavengers, the presence of these ions will scavenge the free radicals and therefore retard the reactions at medium to high pH levels.

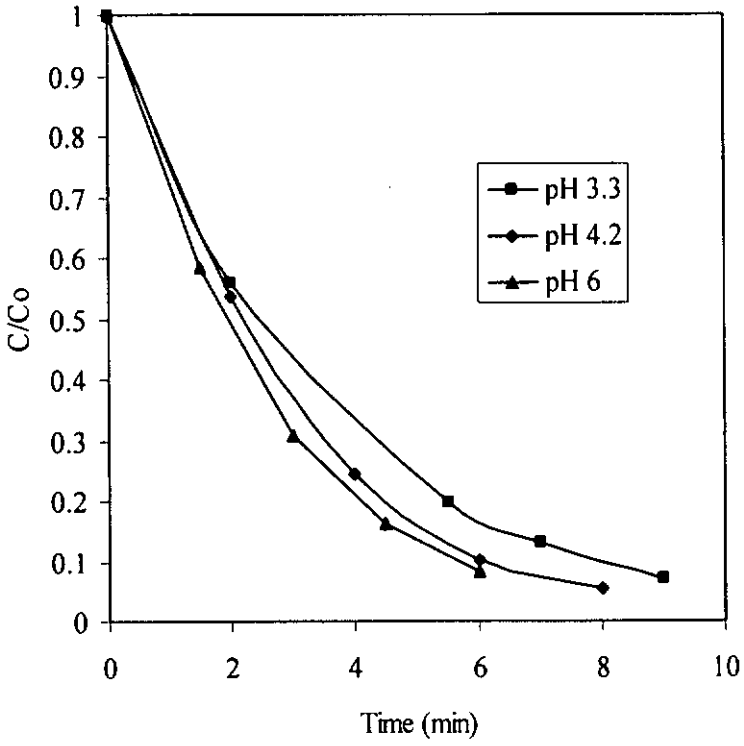

(a)

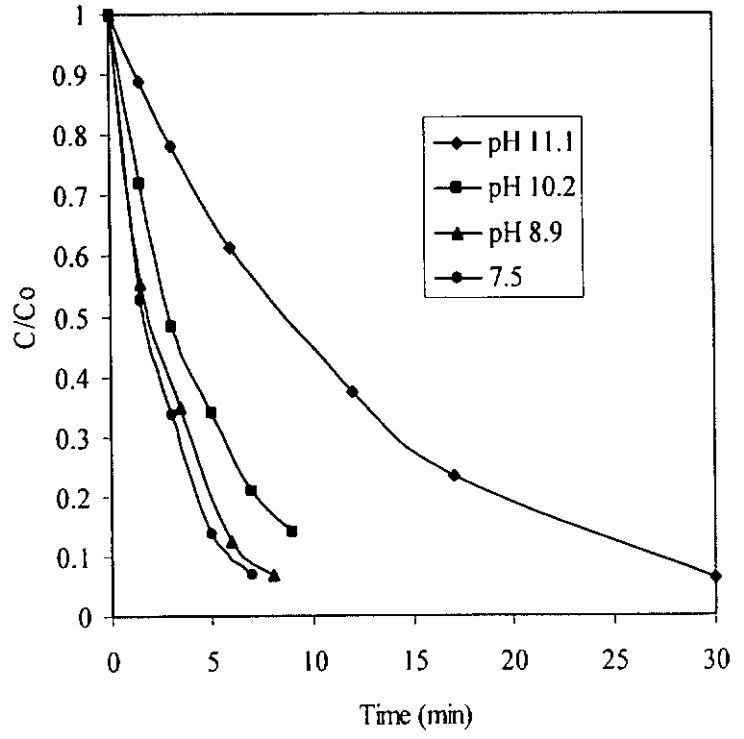

(b)

Figure 3.10 The alachlor decay in H_2O_2-assisted photocatalysis at (a) low (3.3 to 6.0) and (b) high initial pH levels (7.5 to 11.1).

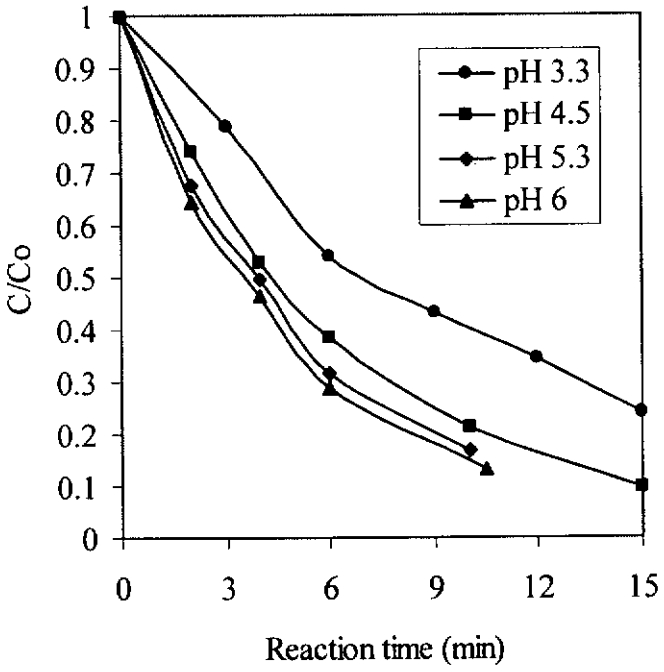

(a)

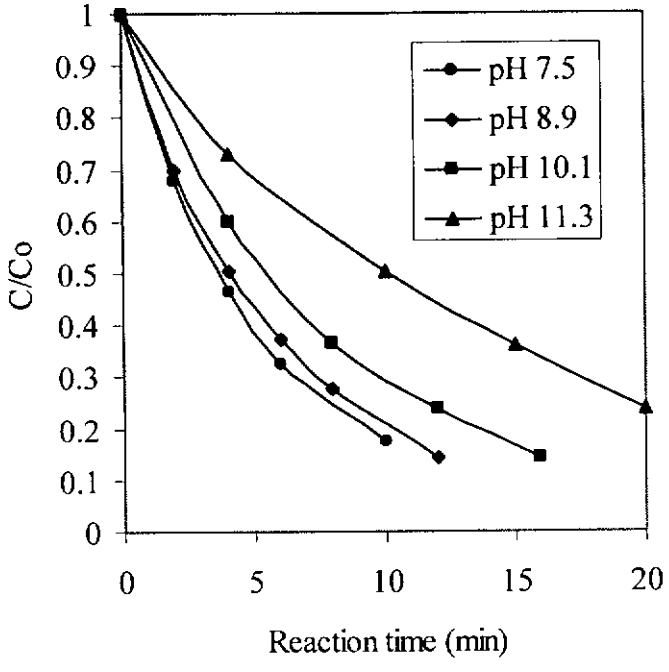

(b)

Figure 3.11 The H_2O_2-assisted photocatalysis of dicamba at (a) low (3.3 to 6.0) and (b) high initial pH levels (7.5 to 11.3).

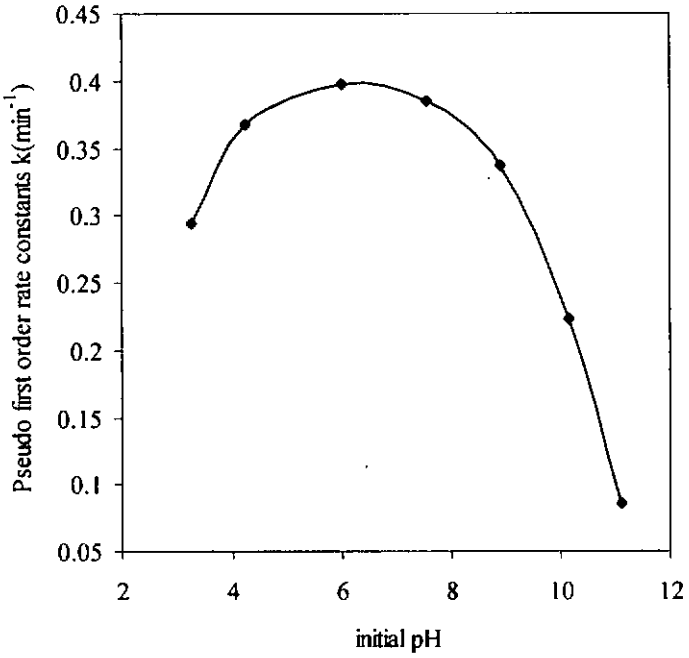

(a)

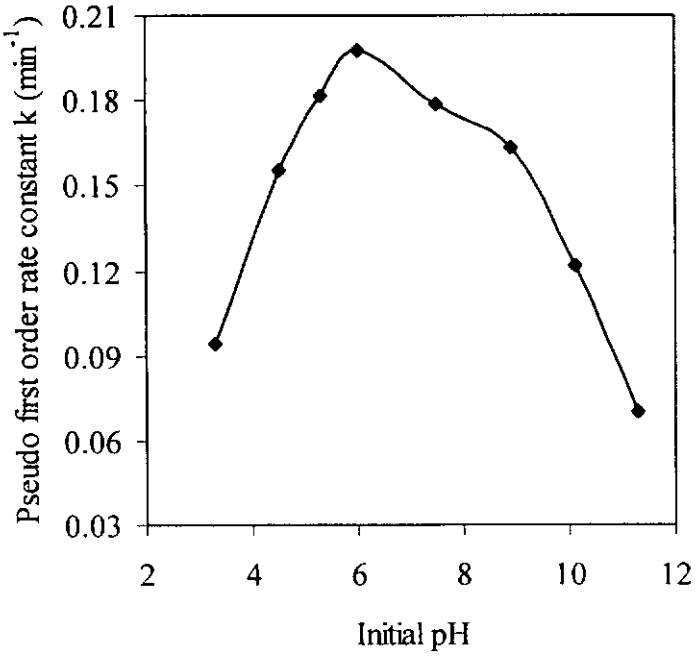

(b)

Figure 3.12 Variation of photocatalytic decay rate of (a) alachlor and (b) dicamba at different initial pH levels at 300 nm of UV with 4.94 mmol/L of H_2O_2.

3.8 The Mechanism of Photocatalytic Decay of Alachlor

GC-MS analysis has been used a lot in the intermediate studies, however, a solvent extraction and/or sample derivatization procedure was usually required, and the escaping of some polar intermediates from the MS detection was inevitable. Therefore, the identification of intermediates in this study was achieved by using the most recent LC-MS to avoid the problem. The protonated alachlor and its reaction intermediates [$M+H^+$] were monitored through out the reaction. Under the current experimental setting, the intensity (in the order of 10^5 to 10^6 relative abundance) of detected ion peaks in full scan mode MS was achieved to detect the decay of alachlor and the generation/decay of reaction intermediates. A total of eight major intermediates were identified in the alachlor photocatalysis at a UV illumination of 300 nm by interpreting and organizing the possible degradation mechanisms from analogous studies (Moza et al., 1992; Peñuela and Barceló, 1996; Konstantinou et al., 2002), the evolution profiles of different degradation products, and the results of double mass analysis (MS/MS). The MS/MS was carried out for the purpose of obtaining more information about the structure of the intermediates, which aided in identification of intermediates. Alachlor and the eight intermediates were subjected to MS/MS analysis. The results including the mass of protonated ion ([$M+H^+$]) of the daughter compounds, the relative abundances, the collision energy applied, and the proposed fragments are summarized in Table 3.2, where the intermediates were presumably subjected to cleavage of the side chains attached to the nitrogen atom and the aromatic ring. The common fragmentation pattern includes loss of mass units of 18, 28, 32, and 44 corresponding to the loss of H_2O, $CHCH_3$, CH_3OH, and $CHOCH_3$ respectively.

Figure 3.13 illustrates the proposed degradation mechanism of the photocatalytic process, in which the decay pathways included dechlorination, hydroxylation, dealkylation, scission of C-O bond, and N-dealkylation. The results have been compared to those from previous research with analogous degradation mechanisms such as alachlor photocatalysis (Moza et al., 1992; Peñuela and Barceló, 1996) and photolysis/photocatalysis of a similar herbicide, propachlor (Konstantinou et al., 2001, 2002), which verify our findings.

For specific intermediates, compounds 1 and 3 are considered to be the major primary intermediates in the process. For compound 1, hydroxyl free radicals react rapidly at unsaturated carbons (Draper and Crosby, 1984), and hydroxyl aromatic products were often found to be the initial oxidation products for the degradation of aromatic compounds in a free radical-based (HO·) oxidation processes (Brezová 1991; Galindo 2000; Wang and Hong, 2000). In addition, as the aromatic ring is electron-rich in nature, the electrophilic attack of the aromatic ring of alachlor by hydroxyl radicals formed compound 1 (Moza et al., 1992). The subsequent loss of an ethyl group on the aromatic rings of compound 1 formed compound 2. Dealkylation was initiated by hydrogen abstraction and normally observed in hydroxyl radical reactions (Draper and Crosby, 1984). The dechlorination and hydroxylation of alachlor formed compound 3 (Peñuela and Barceló, 1996), in which the photodechlorination has been suggested to be a major pathway in a UV photolysis process (Chu, 1999). The scission of the C-O bond of compound 2 formed compound 4.

The deethylation of alachlor formed compound 5 and the subsequent scission of the C-O bond formed compound 6. The dechlorination and N-dealkylation (or scission of N-C bond) of compounds 6 and 4 are observed and generate compounds 8 and 7, respectively. An analogous N-dealkylation mechanism was previously reported in the photocatalytic degradation of propachlor (Konstantinou et al., 2002), pendimethalin (Pandit et al., 1995) and atrazine (Pelizzetti et al., 1990).

Table 3.2 Summary of MS/MS analysis showing the daughter ions, relative abundances, collision energy applied, and proposed fragments.

Protonated parent ion		$[M+H^+]$ of major daughter ions	Collision energy	Proposed fragments	Proposed fragments	Proposed fragments
$[M+H^+]$	Compound no.	(Relative abundances in %)	(eV)	for 1st daughter ion	for 2nd daughter ion	for 3rd daughter ion
270	Alachlor	238(100%)	20	CH_3OH		
286	1	268(36%), 254(100%), 242(45%)	20	H_2O	CH_3OH	$CHOCH_3$
258	2	240(30%), 226(85%)	26	H_2O	CH_3OH	
252	3	234(6%), 220(13%), 176(100%)	25	H_2O	CH_3OH	$HOCH_2$+ CH_2OCH_3
244	4	226(95%), 195(10%)	27	H_2O	$ClCH_2$	
242	5	210(100%), 198(46%)	27	CH_3OH	$CHOCH_3$	
212	6	180(100%), 168(46%)	22	CH_3+ OH	CH_3+ CH_2CH_3	
180	7	163(20%), 152(50%), 134(28%)	26	OH	CH_2CH_3	OH + CH_2CH_3
163	8	147(100%), 134(12%)	26	CH_3	CH_2CH_3	

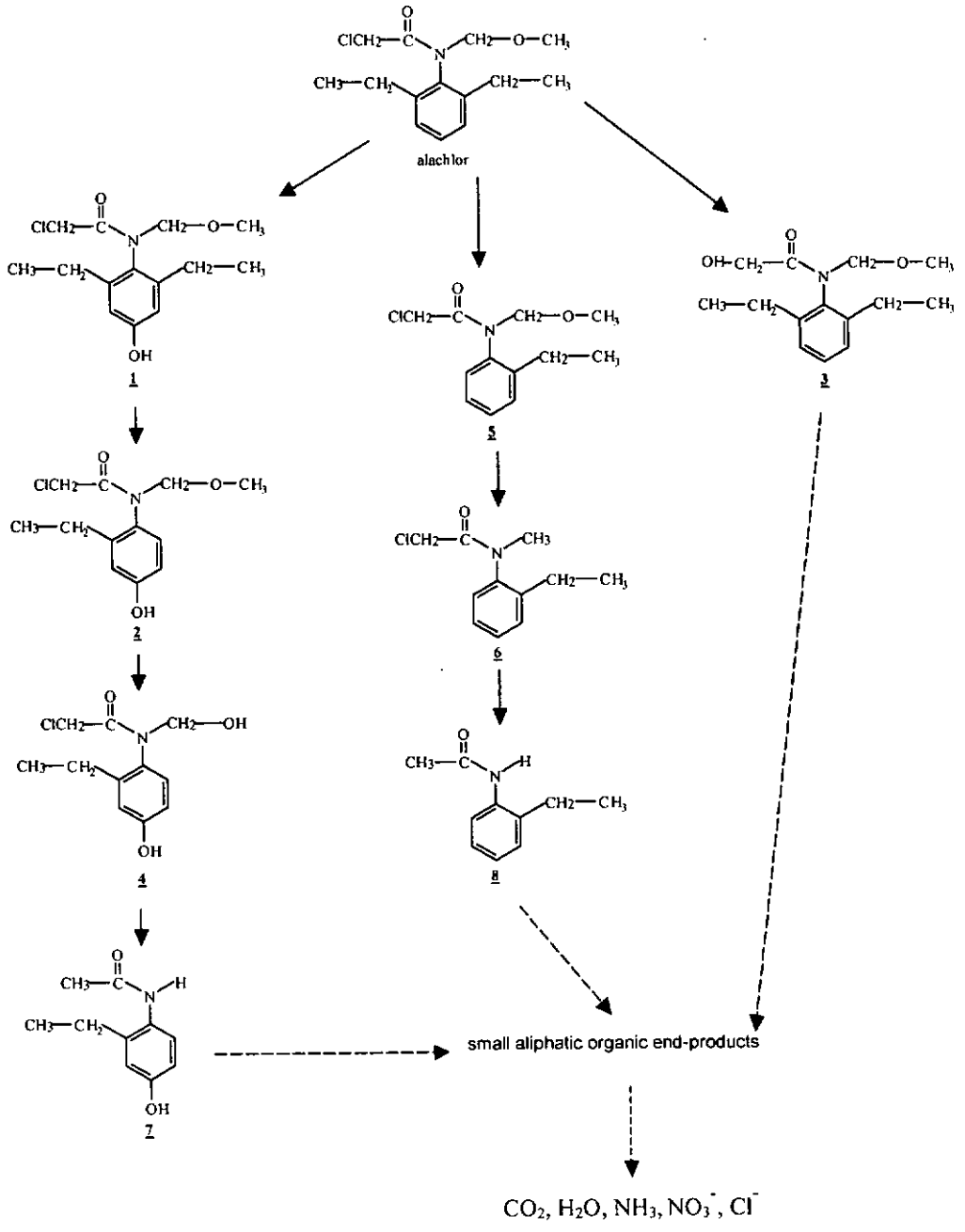

Figure 3.13 Proposed degradation mechanism of alachlor photocatalysis.

3.9 Verification of the proposed degradation pathways in alachlor photocatalysis

The proposed mechanism was further verified by Figure 3.14, which shows the decay and generation of alachlor and the eight identified reaction intermediates during the photocatalytic reaction in terms of the protonated ion $[M+H^+]$ intensity. A study of the evolution profiles offers useful information in supporting the proposed mechanism. For instance, in Figure 3.14, the decay of alachlor leads to the generation of primary intermediates such as compounds 1 and 5, whereas the decay of these two primary intermediates generates secondary intermediates such as compounds 2 and 6, respectively. Compounds 7 and 8 are apparently resistant to free radical attack, as their ion intensity maintained at certain levels until at an extended reaction time of 96.5 min.

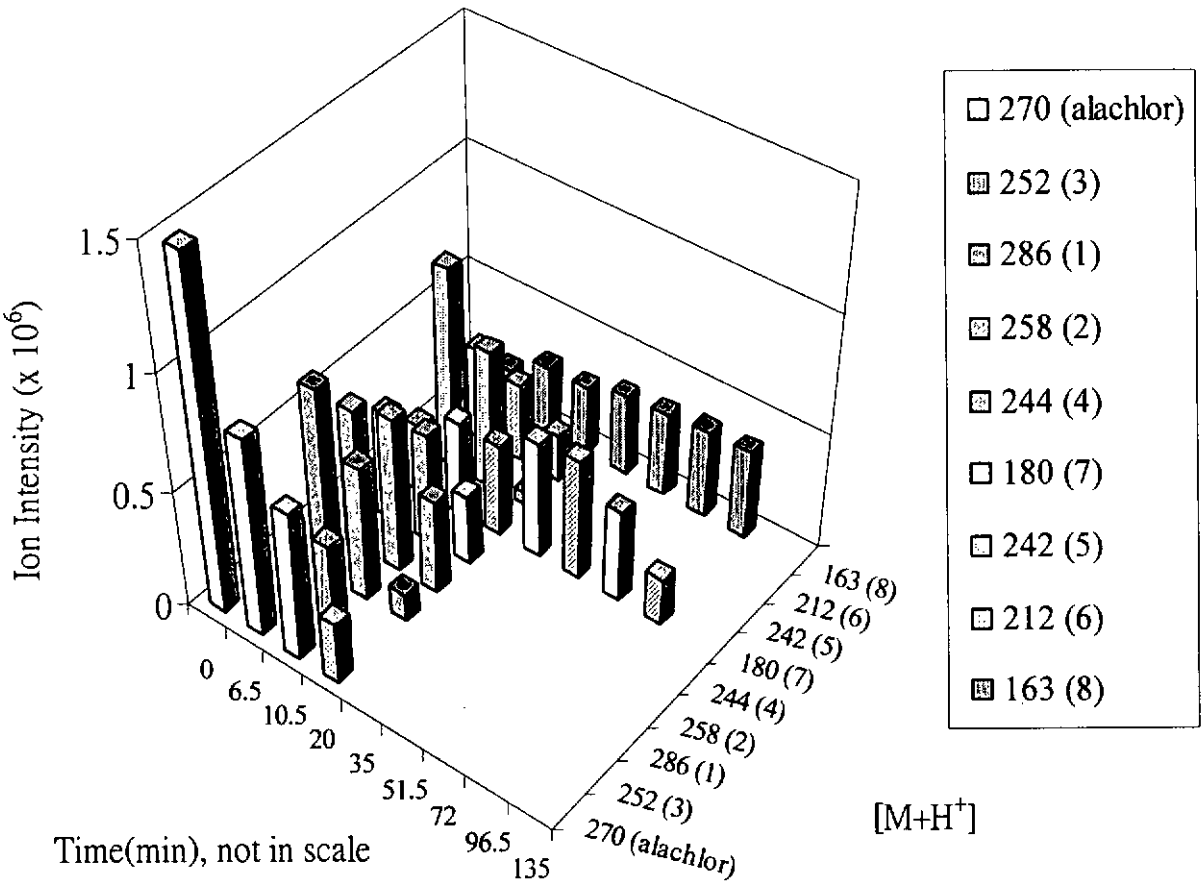

Figure 3.14. The variation of protonated ion intensity of alachlor and the reaction intermediates during the alachlor photocatalysis, where the initial pH level is 6.

3.10 The mechanism of decay of alachlor in H_2O_2-assisted photocatalysis

Similar to the analysis of the degradation mechanism of alachlor in photocatalysis, a total of eleven major intermediates were identified in the H_2O_2-assisted alachlor photocatalysis at 300 nm, in which five intermediates were new. The evolution profiles of different degradation products, and the results of double mass spectrum (MS/MS). The MS/MS results, including the mass of protonated ion ([M+H$^+$]) of the daughter compounds, the relative abundances, the collision energy applied, and the proposed fragments are summarized in Table 3.3, where the intermediates were presumably subjected to cleavage of the side chains

attached to the nitrogen atom and the aromatic ring. The common fragmentation pattern includes loss of mass units of 18, 28, 32, 44, 49, and 77, corresponding to the loss of H_2O, $CHCH_3$, CH_3OH, $CHOCH_3$, $ClCH_2$ and $ClCH_2CO$ respectively.

Figure 3.15 illustrates the proposed degradation mechanism of the H_2O_2-assisted photocatalytic process, in which the decay pathways included dechlorination, hydroxylation, cyclization, dealkylation, scission of C-O bond, and N-dealkylation. Compounds 1 and 3 are considered to be the major primary intermediates in the process. The electrophilic attack of the aromatic ring of alachlor by hydroxyl radicals formed compound 1. The subsequent loss of an ethyl group on the aromatic rings of compound 1 formed compound 2. The dechlorination and hydroxylation of alachlor formed compound 3. The scission of the C-O bonds of compounds 2 and 3 formed compounds 4 and 6, respectively. The different scission positions of the C-O bond of compound 5 formed compounds 10 and 7.

Another primary intermediate, compound 8, formed through a cyclization process, was also characterized by (Chiron et al., 1995) as a major intermediate in the photolysis of alachlor. Dealkylation from the benzene ring of alachlor and compound 4, resulting in the formation of compounds 5 and 9 respectively. The N-dealkylation of compounds 7 and 10 are observed and generate compound 11.

Table 3.3 Summary of MS/MS analysis showing the daughter ions, relative abundances, collision energy applied, and proposed fragments.

Protonated parent ion		$[M+H^+]$ of major daughter ions	Collision energy	Proposed fragments	Proposed fragments	Proposed fragments
$[M+H^+]$	Compound no.	(relative abundances in %)	(eV)	for 1st daughter ion	for 2nd daughter ion	for 3rd daughter ion
270	alachlor	238(100%)	20	CH_3OH		
286	1	268(40%), 254(45%), 242(65%)	23	H_2O	CH_3OH	$CHOCH_3$
258	2	240(35%), 226(60%)	20	H_2O	CH_3OH	
252	3	234(5%), 220(12%), 176(100%)	23	H_2O	CH_3OH	$HOCH_2$+ CH_2OCH_3
244	4	226(100%), 195(10%)	27	H_2O	$ClCH_2$	
242	5	198(100%), 147(50%)	25	$CHOCH_3$	CH_2OCH_3 + $ClCH_2$	
238	6	220(55%), 162(88%)	25	H_2O	$HOCH_2CO$+ OH	
228	7	196(40%), 151(100%)	20	CH_3 + OH	$ClCH_2CO$	
219	8	201(100%), 191(5%)	25	H_2O	$CHCH_3$	
216	9	198(80%), 161(60%)	25	H_2O	HCl + H_2O	
212	10	180(75%) and 168(100%)	25	CH_3+ OH	CH_3+ CH_2CH_3	
198	11	180(75%) and 170(30%)	30	H_2O	$CHCH_3$	

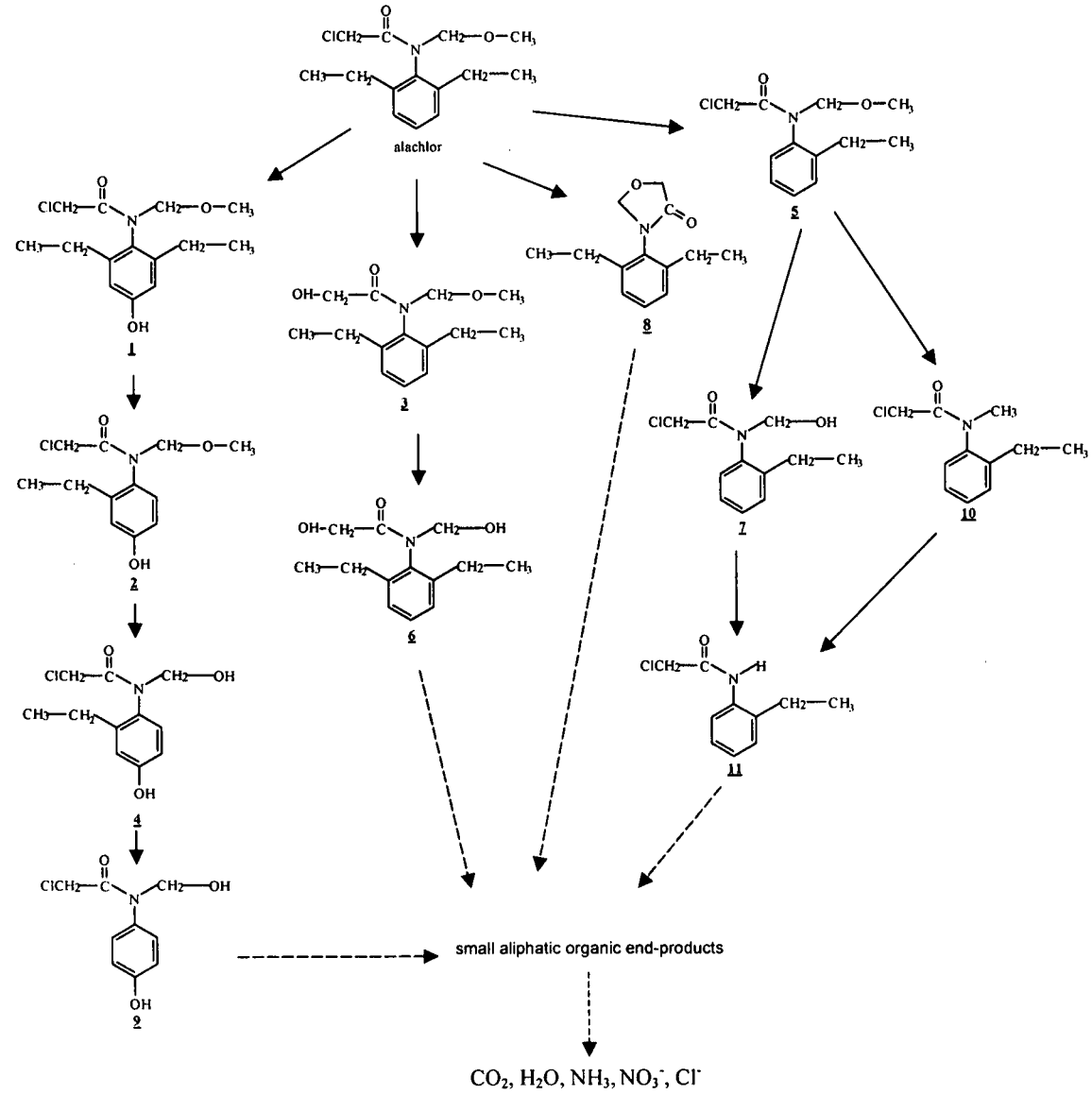

Figure 3.15 Proposed degradation mechanism of H_2O_2-assisted alachlor photocatalysis.

3.11 Verification of the proposed degradation pathways in H_2O_2-assisted alachlor photocatalysis

The proposed mechanism was further verified by Figure 3.16, which shows the decay and generation of alachlor, the eleven identified reaction intermediates, and some unidentified low-molecular-weight intermediates and/or end products

during the hydrogen peroxide catalyzed photocatalytic reaction in terms of the protonated ion [$M+H^+$] intensity. A study of the evolution profiles offers useful information in supporting the proposed mechanism. For instance, in Figure 3.16, the decay of alachlor leads to the generation of primary intermediates such as compounds 1 and 3, whereas the decay of these two primary intermediates generates secondary intermediates such as compounds 2 and 6, respectively. The gradual increases of the ion intensity of the small molecular weight compounds (*i.e.* the protonated masses of 60, 83 and 100) were probably the polar end products formed after the cleavage of the benzene ring. These end products are apparently resistant to free radical attack, as their ion intensity was maintained at high levels even at an extended reaction time of 95 min.

TOC analysis was carried out simultaneously with LC-MS analysis to verify the conversions (decay/generation) of different molecular size species (see Figure 3.17). The decay of TOC could be divided into three stages: the first stage was the lag phase, where the TOC reduction was insignificant because the dominant reaction was the decay of alachlor to primary intermediates with high molecular weights. The lag phase was followed by a mild TOC decay, in which 90% of the alachlor was decayed; the decay of high molecular weight intermediates (to lower ones) was initiated and became the dominant process. In the final stage, the TOC decay rate increased significantly, indicating that the dominant decaying species were small molecules. About 90% of the TOC was removed (or mineralized) at 95 min.

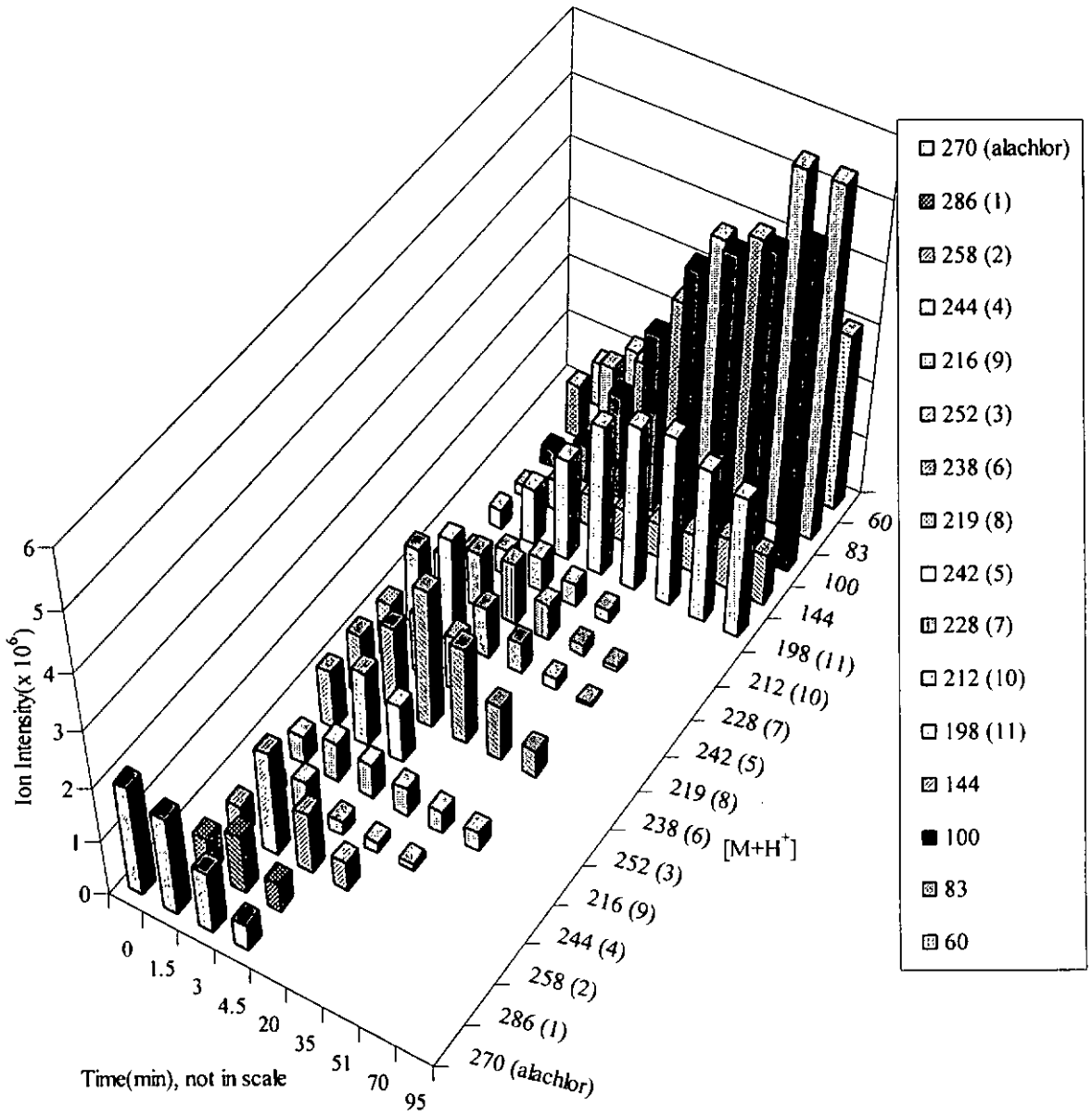

Figure 3.16 The variation of protonated ion intensity of alachlor, the reaction intermediates and end products during the H_2O_2-assisted photocatalysis at 300 nm, where the $[H_2O_2]$ is 4.94 mmol/L and the initial pH level is 6.

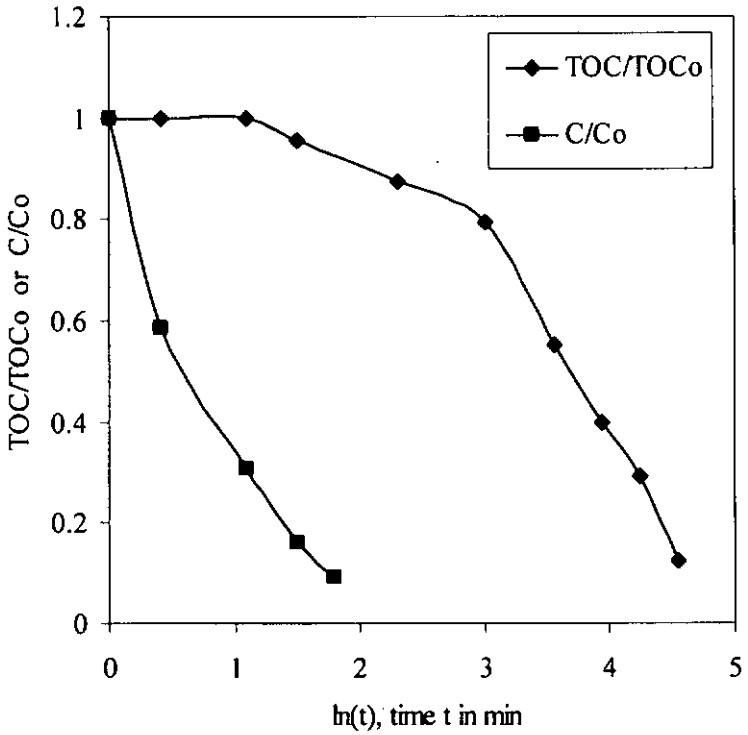

Figure 3.17 Comparison of the photocatalytic decay of alachlor and TOC at 300 nm, where the [H_2O_2] is 4.94 mmol/L and the initial pH level is 6.

Chapter 4: Conclusion

The pseudo first-order decay kinetics of alachlor and dicamba were observed for both direct photolysis and photocatalysis using three different monochromatic UV lamps at 254, 300 and 350 nm. TiO_2 -P25 was shown to be an effective photocatalyst compared to a TiO_2 -BDH, due to its relative high surface area and small particle size. A comparison of the direct photolysis and photocatalysis quantum yields showed that direct photolysis of alachlor and dicamba was always the dominant degradation mechanism even if the TiO_2 was involved, which suggests that the photocatalytic reaction was not effective at 254 nm. However, very high photocatalysis quantum yields were obtained by using near UV ranges of light sources, such as 300 nm.

Photocatalytic degradation rates of alachlor and dicamba increased with dosage of TiO_2, but overdoses may cause rate retardation because the effect of light scattering and attenuation becomes significant. Photocatalytic reactions were slightly enhanced in alkaline solutions due to the increase of hydroxide ions and photocatalytic rates of dicamba were increased with pH at low pH range, but the reaction was gradually retarded at alkaline medium due to effect of charges repulsion. The different sources of protons resulted in different degrees of rate retardation due to the different counter anions involved. Anions such as SO_4^{2-}, NO_3^- and $H_2PO_4^{2-}$ could inhibit the coupling of target compounds with TiO_2 particles, and therefore retard the reaction rates.

Adding H_2O_2 to the photocatalysis of alachlor and dicamba has been examined at two different near UV wavelengths, in which the different

characteristics of H_2O_2 in improving and retarding the reaction rates were quantified and discussed. The use of H_2O_2 in the photocatalysis process is not recommended at 350 nm due to the low molar absorptivity of H_2O_2. However, in the H_2O_2-assisted photocatalysis of alachlor and dicamba at 300 nm UV irradiation, an optimal condition of 4.94 mmol/L H_2O_2 and initial pH level of 6 was found, where an additional 3.3 and 2.4 times rate enhancement was achieved for alachlor and dicamba respectively compared to the sole photocatalysis.

Because almost 3-fold rate enhancement could be achieved for the two target herbicides by using the UV 300 nm mediated H_2O_2-assisted photocatalysis, it is therefore expected that the treatment process should be very useful for practical application. In particular, when technology is mature enough such that the TiO_2 particles could be successfully immobilized onto certain substrates, the treatment process should have high potential in drinking water purification and wastewater treatment.

The use of LC-ESI-MS/MS enabled us to determine the hydrophilic intermediates directly and hence improved the chances of intermediates identification. The possible reaction mechanisms of the photocatalysis or H_2O_2-assisted photocatalysis of alachlor associated with the identification of intermediates, end products, and degradation/generation pathways were proposed and verified via the examinations of LCMS, MS/MS and TOC information. The TOC analysis revealed the different degradation stages of the reaction. The findings of this study would certainly enrich our understanding about the degradation process of alachlor.

References

1. Aceituno M, Stalikas CD, Lunar L, Rubio S, Pérez-Bendito D. H_2O_2/TiO_2 photocatalytic oxidation of metol. Identification of intermediates and reaction pathways. Wat Res 2002;36:3582-3592
2. Alfano OM, Cabrera MI, Cassano AE. Photocatalytic Reactions involving hydroxyl radical attack: I. reaction kinetics formulation with explicit photon absorption effects. J Catal 1997;172:370-379
3. Andreozzi R, Caprio V, Insola A, Marotta R. Advanced oxidation processes (AOP) for water purification and recovery. Catal Today 1999;53: 51-59.
4. Augugliaro V, Davì E, Palmisano L, Schiavello M, Sclafani A. Influence of hydrogen peroxide on the kinetics of phenol photodegradation in aqueous titanium dioxide dispersion. Appl Catal 1990;65:101-116
5. Augugliaro V, Loddo V, Palmisano L, Schiavello M. Performance of heterogeneous photocatalytic systems: influence of operational variables on photoactivity of aqueous suspension of TiO_2. J Catal 1995;153:32-40
6. Battaglin WA, Furlong ET, Burkhardt MR, Peter CJ. Occurrence of sulfonylurea, sulfonamide, imidazolinone, and other herbicides in rivers, reservoirs and ground water in the Midwestern United States, 1998. Sci Total Environ 2000;248:123-133
7. Bekbölet M, Balcioglu I. Photocatalytic degradation kinetics of humic acid in aqueous TiO_2 dispersions: the influence of hydrogen peroxide and bicarbonate ion. Water Sci Technol 1996;34:73-80

8. Bekbölet M, Çeçen F, Özkösemen G. Photocatalytic oxidation and subsequent adsorption characteristics of humic acids. Water Sci Technol 1996;34:65-72

9. Bianco-Prevot A, Fabbri D, Pramauro E, Morales-Rubio A, de la Guardia M. Continuous monitoring of photocatalytic treatments by flow injection. Degradation of dicamba in aqueous TiO_2 dispersions. Chemosphere 2001;44: 249-255

10. Bianco-Prevot A, Vincenti M, Bianciotto A, Pramauro E. Photocatalytic and photolytic transformation of chloramben in aqueous solutions. Appl Catal B: Environ 1999;22:149-158

11. Bianco-Prevot A, Vincenti M, Bianciotto A, Pramauro E. Photocatalytic and photolytic transformation of chloramben in aqueous solutions. Appl Catal B Environ 1999;22:149-158

12. Blount MC, Kim DH, Falconer JL. Transparent thin-film TiO_2 photocatalysts with high activity. Environ Sci Technol 2001;35:2988-2994

13. Brezová V, Čeppan M, Brandšteterová E, Breza M, Lapčík L. Photocatalytic hydroxylation of benzoic acid in aqueous titanium dioxide suspension. J Photochem Photobiol A Chem 1991;59:385-391

14. Burrows HD, Canle L M, Santaballa JA, Steenken S. Reaction pathways and mechanisms of photodegradation of pesticides. J Photochem Photobiol B: Biol 2002;67:71-108

15. Chen HY, Zahraa O, Bouchy M. Inhibition of the adsorption and photocatalytic degradation of an organic contaminant in an aqueous

suspension of TiO_2 by inorganic ions. J Photochem Photobiol A Chem 1997;108:37-44

16. Chen TF, Doong RA, Lei WG. Photocatalytic degradation of parathion in aqueous TiO_2 dispersion: the effect of hydrogen peroxide and light intensity. Water Sci Tech 1998;37:187-194
17. Chiron S, Abian J, Ferrer M, Sanchezbaeza F, Messeguer A, Barcelo D. Comparative photodegradation rates of alachlor and bentazone in natural-water and determination of breakdown products. Environ Toxicol Chem 1995;14:1287-1298
18. Chiron S, Fernandez-Alba A, Rodriguez A, Garcia-Calvo E. Pesticide chemical oxidation: state-of-the-art. Water Res 2000;34:366-377
19. Chiron S, Fernandez-Alba AR, Rodriguez A. Pesticide chemical oxidation processes: an analytical approach. Trend Anal Chem 1997;16:518-527.
20. Chu W, Choy WK. The mechanisms of rate enhancing and quenching of trichloroethene photodecay in the presence of sensitizer and hydrogen sources. Water Res 2002;36:2525-2532
21. Chu W, Jafvert CT, Diehl CA, Marley K, Larson RA. Phototransformations of polychlorobiphenyls in Brij 58 micellar solutions. Environ Sci Technol 1998; 32:1989-1993
22. Chu W, Jafvert CT. Photodechlorination of polychlorobenzene congeners in surfactant micelle solutions. Environ Sci Technol 1994;28:2415-2422
23. Chu W, Ma CW. Quantitative prediction of direct and indirect dye ozonation kinetics. Water Res 2000;34:3153-3160

24. Chu W. Modeling the quantum yields of herbicide 2,4-D decay in UV/H_2O_2 process. Chemosphere 2001;44:935-941

25. Chu W. Photodechlorination mechanism of DDT in a UV/surfactant system. Environ Sci Technol 1999;33:421-425

26. Connor PA, McQuillan AJ. Phosphate adsorption onto TiO_2 from aqueous solutions: An in situ internal reflection infrared spectroscopic study. Langmuir 1999;15:2916-2921

27. Cornish BJPA, Lawton LA, Robertson PKJ. Hydrogen peroxide enhanced photocatalytic oxidation of microcystin-LR using titanium dioxide. Appl Catal B: Environ 2000;25:59-67

28. Dillert R, Fornefett I, Siebers U, Bahnemann D. Photocatalytic degradation of trinitrotoluene and trinitrobenzene: influence of hydrogen peroxide. J Photochem Photobiol A Chem 1996;94:231-236

29. Dionysiou DD, Suidan MT, Bekou E, Baudin I, Laîné JM. Effect of ionic strength and hydrogen peroxide on the photocatalytic degradation of 4-chlorobenzoic acid in water. Appl Catal B: Environ 2000;26:153-171

30. Doong RA, Chang WH. Photodegradation of parathion in aqueous titanium dioxide and zero valent iron solutions in the presence of hydrogen peroxide. J Photochem Photobiol A Chem 1998;116:221-228

31. Doong RA, Maithreepala RA, Chang SM. Heterogeneous and homogeneous photocatalytic degradation of chlorophenols in aqueous titanium dioxide and ferrous ion. Water Sci Technol 2000;42:253-260

32. Draper WM, Crosby DG. Solar Photooxidation of pesticides in dilute hydrogen peroxide. J Agric Food Chem 1984;32:231-237

33. Galindo C, Jacques P, Kalt A. Photodegradation of the aminoazobenzene acid orange 52 by three advanced oxidation processes: UV/H_2O_2, UV/TiO_2 and VIS/TiO_2 Comparative mechanistic and kinetic investigations. J Photochem Photobiol A Chem 2000;130:35-47

34. Gao R, Stark J, Bahnemann D, Rabani J. Quantum yields of hydroxyl radicals in illuminated TiO_2 nanocrystallite layers. J Photochem Photobiol A Chem 2002;248:387-391

35. Grover R, Cessna AJ (Eds.), Environmental Chemistry of herbicides, CRC Press, Boca Raton, FL, 1991.

36. Ilisz I, Föglein K, Dombi A. The photochemical behavior of hydrogen peroxide in near UV-irradiated aqueous TiO_2 suspensions. J Mol Catal 1998;135:55-61

37. Jardim WF, Moraes SG, Takiyama MK. Photocatalytic degradation of aromatic chlorinated compounds using TiO_2: toxicity of intermediates. Water Res 1997;31:1728-1732

38. Jenny B, Pichat P. Determination of the Actual Photocatalytic Rate of H_2O_2 Decomposition over suspended TiO_2. Fitting to the Langmuir-Hinshelwood Form. Langmuir 1991;7:947-954

39. Konstantinou IK, Albanis TA. Photocatalytic transformation of pesticides in aqueous titanium dioxide suspensions using artificial and solar light: intermediates and degradation pathways. Appl Catal B: Environ 2002;1310:1–17

40. Konstantinou IK, Sakka VA, Albanis TA. Photocatalytic degradation of propachlor in aqueous TiO_2 suspensions. Determination of the reaction

pathway and identification of intermediate products by various analytical methods. Water Res 2002; 36:2733-2742

41. Konstantinou IK, Zarkadis AK, Albanis TA. Photodegradation of selected herbicides in various natural waters and soils under environmental conditions. J Environ Qual 2001;30:121-130
42. Larson SJ, Gilliom RJ, Capel PD. Pesticides in streams of the United States- initial results from the National Water-Quality Assessment Program, U.S. Geological Survey Water-Resources Investigations Report 98-4222: 1999, California, pp.16 & 75
43. Lu MC, Chen JN. Pretreatment of pesticide wastewater by photocatalytic oxidation. Water Sci Tech 1997;36:117-122
44. Lu MC, Roam GD, Chen JN, Huang CP. Photocatalytic oxidation of dichlorvos in the presence of hydrogen peroxide and ferrous ion. Water Sci Tech 1994;30:29-38
45. Makarova OV, Rajh T, Thurnauer MC. Surface modification of TiO_2 nanoparticles for photochemical reduction of nitrobenzene. Environ Sci Technol 2000;34:4797-4803
46. Malato S, Blanco J, Vidal A, Richter C. Photocatalysis with solar energy at a pilot-plant scale: an overview. Appl Catal B: Environ 2002;37:1-15.
47. Manilal VB, Haridas A, Alexander R, Surender GD. Photocatalytic treatment of toxic organics in wastewater – toxicity of photodegradation products. Water Res 1992;26:1035-1038
48. Minero C, Pelizzetti E, Pichat P, Sega M, Vincenti M. Formation of Condensation Products in Advanced Oxidation Technologies: The

Photocatalytic Degradation of Dichlorophenols on TiO_2. Environ Sci Technol 1995;29:2226-2234

49. Moza PN, Hustert K, Pal S, Sukul P. Photocatalytic decomposition of pendimethalin and alachlor. Chemosphere 1992;25: 1675-1682
50. Nargiello M, Herz T. Physical-chemical characteristics of P-25 making it extremely suited as the catalyst in photodegradation of organic compounds. In: Ollis, D.F., and H., Al-Ekabi. (Eds.). Proceedings of the 1st international conference on TiO_2 photocatalytic purification and treatment of water and air. Elsevier Science, Amsterdam, 1993, pp.801-807
51. Ollis DF, Pelizzetti E, Serpone N. Destruction of water contaminants. Environ Sci Technol 1991;25:1523-1529
52. Ollis DF. Contaminant degradation in water. Environ Sci Technol 1985;19: 480-484
53. Palmisano L, Augugliaro V, Campostrini R, Schiavello M. A proposal for the quantitative assessment of heterogeneous photocatalytic processes. J Catal 1993;143:149-154
54. Pandit GK, Pal S, Das AK. Photocatalytic degradation of pendimethalin in the presence of titanium dioxide. J Agric Food Chem 1995;43:171-174
55. Pavel EW, Lopez AR, Berry DF, Smith EP, Reneau RBJr, Mostaghimi S. Anaerobic degradation of dicamba and metribuzin in riparian wetland soils. Wat Res 1999;33:87-94

56. Pelizzetti E, Maurino V, Minero C, Carlin V, Pramauro E, Zerbinati O, Tosato ML. Photocatalytic degradation of atrazine and other s-triazine herbicides. Environ Sci Technol 1990;24:1559-1565

57. Peñuela GA, Barceló D. Application of C-18 disks followed by gas chromatography techniques to degradation kinetics, stability and monitoring of endosulfan in water. J Chromatogr A 1998;795:93-104

58. Peñuela GA, Barceló D. Comparative degradation kinetics of alachlor in water by photocatalysis with $FeCl_3$, TiO_2 and photolysis, studied by solid-phase disk extraction followed by gas chromatographic techniques. J Chromatogr A 1996;754: 187-195

59. Peñuela GA, Barceló D. Comparative photodegradation study of atrazine and desethylatrazine in water samples containing titanium dioxide/hydrogen peroxide and ferric chloride/hydrogen peroxide. J Aoac Int 2000;83:53-60

60. Peñuela GA, Barceló D.Photosensitized degradation of organic pollutants in water: processes and analytical applications. Trend Anal Chem 1998;17:605-612

61. Potter TL, Carpenter TL. Occurrence of alachlor environmental degradation products in groundwater. Environ Sci Technol 1995;29:1557-1563

62. Ranjit KT, Willner I, Bossmann SH, Braun AM. Lanthanide Oxide Doped Titanium Dioxide Photocatalysts: Effective Photocatalysts for the Enhanced Degradation of Salicylic Acid and t-Cinnamic Acid. J Catal 2001;204:305–313

63. San N, Hatipoğlu A, Koçtürk G, Çınar Z. Photocatalytic degradation of 4-nitrophenol in aqueous TiO_2 suspensions: Theoretical prediction of the intermediates. J Photochem Photobiol A: Chem 2002;146:189–197

64. Sánchez L, Peral J, Domenèch X. Photocatalyzed destruction of aniline in UV-illuminated aqueous TiO_2 suspensions. Electrochim Acta 1997;42:1877-1882

65. Sarria V, Parra S, Adler N, Péringer P, Benitez N, Pulgarin C. Recent developments in the coupling of photoassisted and aerobic biological processes for the treatment of biorecalcitrant compounds. Catal Today 2002;76;301-315.

66. Smith AE. Breakdown of the herbicide dicamba and its degradation product 3,6-dichlorosalicylic acid in prairie soils. J Agr Food Chem 1974;22:601-605

67. Tang WZ, An H. Photocatalytic Degradation Kinetics and Mechanism of Acid Blue 40 by TiO_2/UV in Aqueous Solution. Chemosphere 1995;31:4171-4183

68. Thurman EM, Ferrer I, Barceló D. Choosing between atmospheric pressure chemical ionization and electrospray ionization interfaces for the HPLC/MS analysis of pesticides. Anal Chem 2001;73:5441-5449

69. Topalov A, Molnár-Gábor D, Kosanić M, Abramović B. Photomineralization of the herbicide mecoprop dissolved in water sensitized by TiO_2. Water Res 2000;34:1473-1478

70. Wang YB, Hong CS. TiO_2-mediated photomineralization of 2-chlorobiphenyl: the role of O_2. Water Res 2000;34:2791-2797

71. Wei TY, Wang YY, Wan CC. Photocatalytic oxidation of phenol in the presence of hydrogen peroxide and titanium dioxide powders. J Photochem Photobiol A Chem 1990;55:115-126

72. Xu Y, Langford CH. Variation of Langmuir adsorption constant determined for TiO_2-photocatalyzed degradation of acetophenone under different light intensity. J Photochem Photobiol A Chem 2000;133:67-71.

73. Yang HG, Li CZ, Gu HC, Fang TN. Rheological behavior of titanium dioxide suspensions. J Colloid Interf Sci 2001;236:96-103

74. Yu JC, Lin J, Kwok RWM. Enhanced photocatalytic activity of $Ti_{1-x}V_xO_2$ solid solution on the degradation of acetone. J Photochem Photobiol A Chem 1997;111:199-203

75. Zang LY, DeHaven J, Yocum A, Qiao G. Determination of alachlor and its metabolites in rat plasma and urine by liquid chromatography-electrospray ionization mass spectrometry. J Chromatogr B 2002;767:93-101.

76. Zhao HT, Jaynes WF, Vance GF. Sorption of the ionizable organic compound, dicamba(3,6-dichloro-2-methoxy benzoic acid), by organo-clays. Chemosphere 1996;33: 2089-2100

Appendix (raw data)

Data for Figure 3.1 The pseudo first-order decay of (a) alachlor and (b) dicamba via direct photolysis and photocatalysis (with TiO2-BDH or TiO2-P25) illuminated at 300 nm, where the TiO2 dosage is 5 mg/L and the initial pH level was 6.

(a) alachlor

UV 300 nm

Time (min)	x 10^{-5} M
0	2.19
9	1.99
15	1.79
25	1.61

UV 300 nm + TiO2-BDH

Time (min)	x 10^{-5} M
0	2.21
9	1.67
15	1.22
25	0.87

UV 300 nm + TiO2-P25

Time (min)	x 10^{-5} M
0	2.21
3	1.45
6.5	0.98
10.5	0.59
15	0.32

(b) dicamba

UV 300 nm

Time (min)	x 10^{-5} M
0	2.22
10	1.77
25	1.14
35	0.82
45.5	0.62

UV 300 nm + TiO2-BDH

Time (min)	x 10^{-5} M
0	2.21
7	1.70
15	1.17
24	0.88
35	0.56

UV 300 nm + TiO2-P25

Time (min)	x 10^{-5} M
0	2.23
2	1.82
4	1.53
6	1.31
11	0.90
16	0.62
25	0.24

Data for Table 3.1 Comparison of direct photolysis and photocatalysis of alachlor and dicamba at different UV wavelengths (the dosage of TiO2 -P25 is 5 mg/L, and the initial pH is 6)

(a) alachlor

UV 254 nm

Time (min)	x 10^{-5} M
0	2.23
3	1.81
6	1.32
10	0.93
12.5	0.73
25	0.25

UV 254 nm + TiO2

Time (min)	x 10^{-5} M
0	2.23
6	1.11
15	0.40
25	0.14

UV 350 nm

Time (min)	x 10^{-5} M
0	2.21
9	2.13
16	2.04
25	1.96

UV 350 nm + TiO2

Time (min)	x 10^{-5} M
0	2.22
6	1.27
15	0.32
25	0.08

(b) dicamba

UV 254 nm

Time (min)	x 10^{-5} M
0	2.18
5	1.44
10	1.03
15	0.65
20	0.45

UV 254 nm + TiO2

Time (min)	x 10^{-5} M
0	2.22
4	1.47
8	1.00
12	0.68
18	0.38

UV 350 nm

Time (min)	x 10^{-5} M
0	2.22
10	1.93
25	1.56
35	1.40
45	1.20

UV 350 nm + TiO2

Time (min)	x 10^{-5} M
0	2.19
4	1.73
6	1.50
16	0.78
24	0.44
30	0.28

Data for Figure 3.2 The pseudo first-order photodecay of (a) alachlor and (b) dicamba at various dosages of TiO_2-P25, where the initial pH level is 6.

(a) alachlor

	25 ppmTiO2
Time (min)	x 10^{-5} M
0	2.20
4	0.53
8	0.14
12	0.05

	50 ppmTiO2
Time (min)	x 10^{-5} M
0	2.21
2	0.59
4	0.17
6	0.05

	75 ppmTiO2
Time (min)	x 10^{-5} M
0	2.21
4	0.53
8	0.14
12	0.04

	100 ppmTiO2
Time (min) (min)	x 10^{-5} M
0	2.20
6	0.37
15	0.03

(b) dicamba

	25 ppmTiO2
Time (min)	x 10^{-5} M
0	2.21
5	0.92
10	0.32
15	0.15

	50 ppmTiO2
Time (min)	x 10^{-5} M
0	2.22
5	0.46
10	0.10
15	0.03

	75 ppmTiO2
Time (min)	x 10^{-5} M
0	2.21
5	0.90
10	0.37
15	0.18

	100 ppmTiO2
Time (min) (min)	x 10^{-5} M
0	2.19
6	0.93
12	0.36
18	0.13

Data for Figure 3.3 Variation of pseudo first-order rate constants with initial pH in photocatalysis of (a) alachlor and (b) dicamba under the illumination of UV 300 nm, with a TiO_2-P25 dosage of 5 mg/L.

(a) alachlor

pH 3.1

Time (min)	x 10^{-5} M
0	2.20
3	1.55
6	1.10
9	0.76
12	0.53
20	0.20

pH 4.4

Time (min)	x 10^{-5} M
0	2.21
4	1.37
8	0.81
12	0.47
16	0.30

pH 6

Time (min)	x 10^{-5} M
0	2.21
1.5	1.89
3	1.47
6.5	0.98
10.5	0.59
15	0.31

pH 11.3

Time (min)	x 10^{-5} M
0	2.20
6	0.94
11	0.44
16	0.18

pH 10.2

Time (min)	x 10^{-5} M
0	2.21
3	1.44
6.5	0.85
9	0.60
12	0.39

pH 8.5

Time (min)	x 10^{-5} M
0	2.22
5	1.24
10	0.60
15	0.29

(b) dicamba

pH 3.3

Time (min)	x 10^{-5} M
0	2.22
12	1.17
16	0.94
20	0.74
25	0.56
30	0.42
35	0.32

pH 4.5

Time (min)	x 10^{-5} M
0	2.20
8	1.21
16	0.83
24	0.45
30	0.33

pH 6

Time (min)	x 10^{-5} M
0	2.22
2	1.81
4	1.53
6	1.31
11	0.89
16	0.62
25	0.24

pH 11.3

Time (min)	x 10^{-5} M
0	2.20
8.5	1.21
12	0.96
16	0.73
24	0.39

pH 8.5

Time (min)	x 10^{-5} M
0	2.23
2	1.73
4	1.42
8	0.96
16	0.47
25	0.22

pH 10.1

Time (min)	x 10^{-5} M
0	2.19
8	1.20
11	0.94
16	0.64
23	0.35

Data for Figure 3.4 The photocatalytic decay of alachlor and TOC at initial pH levels of 3.1, 6.0 and 10.2.

pH 3.1

Time (min)	TOC (mg/L)
0	4.40
6	4.36
12	4.32
20	4.09
35	3.76
50	3.43
70	2.90
89	2.65
130	2.00
180	1.41

pH 6

Time (min)	TOC (mg/L)
0	4.17
6.5	4.11
10.5	4.07
20	3.85
35	3.43
51.5	2.88
72	2.44
96.5	1.99
120	1.56

pH 10.2

Time (min)	TOC (mg/L)
0	4.25
6	4.20
12	4.13
20	3.83
35	3.33
50	2.85
70	2.35
90	2.04
130	1.35

Data for Figure 3.5 Comparison of the photocatalytic decay of dicamba and TOC at 300 nm of UV at initial pH levels of 3.3, 6 and 8.5.

pH 3.3

Time (min)	TOC (mg/L)
0	2.76
12	2.57
20	2.50
35	2.16
50	1.70
70	1.20
90	0.90
110	0.66

pH 6

Time (min)	TOC (mg/L)
0	2.78
12	2.46
20	2.30
35	1.83
50	1.40
70	0.94
90	0.64
110	0.43

pH 8.5

Time (min)	TOC (mg/L)
0	2.86
12	2.43
20	2.21
35	1.77
50	1.29
70	0.84
90	0.55
110	0.36

Data for Figure 3.6 Effect of using different proton sources (HCL, H_2SO_4, H_3PO_4 and HNO_3) on the photocatalytic decay of (a) alachlor and (b) dicamba by 300 nm of UV, with a TiO_2-P25 dosage of 5 mg/L at an initial pH of 3.3.

(a) alachlor

H3PO4

Time (min)	x 10^{-5} M
0	2.22
7	2.09
16	1.83
30	1.51
46	1.18
60	0.76
75	0.46

H2SO4

Time (min)	x 10^{-5} M
0	2.21
6	1.94
15	1.64
25	1.18
35.1	0.69
45	0.40
55.1	0.18

HNO3

Time (min)	x 10^{-5} M
0	2.20
10.5	1.87
17	1.77
30	1.50
47	0.88
57	0.71
71	0.43

HCL

Time (min)	x 10^{-5} M
0	2.21
6	1.14
15	0.37
25	0.09

(b) dicamba

H3PO4

Time (min)	x 10^{-5} M
0	2.21
10	1.54
20	1.22
30	0.97
40	0.74

H2SO4

Time (min)	x 10^{-5} M
0	2.23
10	1.41
20	0.91
30	0.58
40	0.33
57	0.09

HNO3

Time (min)	x 10^{-5} M
0	2.22
10	2.03
20.1	1.80
30	1.80
56	1.79
70.5	1.81

HCL

Time (min)	x 10^{-5} M
0	2.20
4	1.76
8	1.40
12	1.12
16	0.88
30	0.44
40	0.23

Data for Figure 3.7 The photocatalytic decay of alachlor at (a) low (0.05 to 1.24 mmol/L) and (b) high (4.94 to 124.0 mmol/L) H2O2 dosages at 300 nm, where the [TiO2] was 5 mg/L and the initial pH level was 6.

UV 300nm

124 mmol/L

Time (min)	x 10^{-5} M
0	2.21
2	1.31
4	0.78
6.5	0.38
8	0.26

UV 300nm

66.7 mmol/L

Time (min)	x 10^{-5} M
0	2.22
2	1.17
4	0.66
6.5	0.33
8	0.21

UV 300nm

9.88 mmol/L

Time (min)	x 10^{-5} M
0	2.24
1.5	1.28
3	0.69
4.5	0.41
6	0.24

UV 300nm

4.94 mmol/L

Time (min)	x 10^{-5} M
0	2.24
1.5	1.31
3	0.69
4.5	0.36
6	0.21

UV 300nm

0.24 mmol/L

Time (min)	x 10^{-5} M
0	2.18
2.5	1.24
5	0.70
7.5	0.40
10	0.23

UV 300nm

1.24 mmol/L

Time (min)	x 10^{-5} M
0	2.23
1.5	1.32
3	0.72
4.5	0.41
6	0.24

UV 300nm

0.74 mmol/L

Time (min)	x 10^{-5} M
0	2.16
2	1.10
4	0.58
6.5	0.29
8	0.16

UV 300nm

0.049 mmol/L

Time (min)	x 10^{-5} M
0	2.16
2	1.56
4	1.17
6.5	0.78
8	0.62

UV 350nm

1.24	mmol/L
Time (min)	x 10^{-5} M
0	2.24
5	1.30
8	0.85
12	0.52
16	0.38

UV 350nm

0.24	mmol/L
Time (min)	x 10^{-5} M
0	2.24
5	1.28
8	0.84
12	0.52
16	0.38

UV 350nm

0.049	mmol/L
Time (min)	x 10^{-5} M
0	2.25
4	1.19
8	0.78
12	0.48
16	0.35

UV 350nm

0.025	mmol/L
Time (min)	x 10^{-5} M
0	2.25
4	1.08
8	0.71
12	0.44
16	0.32

UV 350nm

124	mmol/L
Time (min)	x 10^{-5} M
0	2.16
6	1.43
12	1.05
18	0.73
24	0.55

UV 350nm

66.7	mmol/L
Time (min)	x 10^{-5} M
0	2.17
5	1.42
10	1.05
15	0.71
20	0.51

UV 350nm

9.88	mmol/L
Time (min)	x 10^{-5} M
0	2.22
5	1.47
10	0.96
15	0.61
20	0.37

UV 350nm

4.94	mmol/L
Time (min)	x 10^{-5} M
0	2.2
4	1.49
8	0.97
12	0.61
16	0.44

Data for Figure 3.8 The photocatalytic decay of dicamba at (a) low (0.049 to 1.24 mmol/L) and (b) high (4.94 to 124 mmol/L) H2O2 dosages by 300 nm of UV at initial pH level of 6.

UV 300nm

1.24	mmol/L
Time (min)	x 10^{-5} M
0	2.2
2	1.47
4	1.00
6	0.72
10.5	0.33

UV 300nm

0.74	mmol/L
Time (min)	x 10^{-5} M
0	2.24
3	1.29
6	0.85
9	0.54
12	0.33

UV 300nm

0.25	mmol/L
Time (min)	x 10^{-5} M
0	2.17
3	1.67
6	1.17
9	0.94
12	0.74
20	0.34

0.049	mmol/L
Time (min)	x 10^{-5} M
0	2.18
3	1.68
6	1.35
9	1.03
15	0.64
25	0.25

UV 300nm

124	mmol/L
Time (min)	x 10^{-5} M
0	2.18
3	1.50
6	1.08
9	0.81
12	0.55
20	0.25

UV 300nm

61.7	mmol/L
Time (min)	x 10^{-5} M
0	2.2
5	1.119
10	0.51
15	0.22
20	0.098

UV 300nm

9.88	mmol/L
Time (min)	x 10^{-5} M
0	2.24
2	1.59
4	1.10
6	0.77
8	0.54
12	0.27

4.94	mmol/L
Time (min)	x 10^{-5} M
0	2.2
2	1.42
4	1.02
6	0.63
10.5	0.29

UV 350nm

1.24	mmol/L
Time (min)	x 10^{-5} M
0	2.2
5	1.84
10	1.32
15	0.98
20	0.72

UV 350nm

0.25	mmol/L
Time (min)	x 10^{-5} M
0	2.14
4	1.65
8	1.29
13	0.96
20	0.72

UV 350nm

0.049	mmol/L
Time (min)	x 10^{-5} M
0	2.15
5	1.63
10	1.17
15	0.87
20	0.64

UV 350nm

0.0025	mmol/L
Time (min)	x 10^{-5} M
0	2.21
4	1.62
8	1.16
13	0.87
20	0.63

UV 350nm

124	mmol/L
Time (min)	x 10^{-5} M
0	2.15
15	1.90
30	1.70
45	1.47

UV 350nm

61.7	mmol/L
Time (min)	x 10^{-5} M
0	2.30
10	2.02
25	1.72
40	1.46
60	1.16

UV 350nm

9.88	mmol/L
Time (min)	x 10^{-5} M
0	2.22
10	1.24
20	0.89
30	0.67
40	0.49

UV 350nm

4.94	mmol/L
Time (min)	x 10^{-5} M
0	2.20
5	1.85
10	1.33
15	1.00
20	0.72

Data for Figure 3.10 The alachlor decay in H2O2-assisted photocatalysis at (a) low (3.3 to 6.0) and (b) high initial pH levels (7.5 to 11.1).

alachlor

pH 11.1

Time (min)	x 10^{-5} M
0	2.18
1.5	1.94
3	1.70
6	1.34
12	0.82
17	0.51
30	0.14

pH 10.2

Time (min)	x 10^{-5} M
0	2.23
1.5	1.61
3	1.07
12.5	0.76
17	0.46
27	0.31

pH 8.9

Time (min)	x 10^{-5} M
0	2.24
1.5	1.24
3.5	0.78
4	0.28
5	0.15

pH 7.5

Time (min)	x 10^{-5} M
0	2.19
3	1.15
5	0.74
7	0.30
18	0.150

pH 6

Time (min)	x 10^{-5} M
0	2.22
2	1.19
4	0.55
6	0.23

pH 4.2

Time (min)	x 10^{-5} M
0	2.22
4	1.19
6	0.55
16	0.23

pH 3.26

Time (min)	x 10^{-5} M
0	2.24
2	1.25
5.5	0.44
7	0.29
9	0.16

Data for Figure 3.11 The H2O2-assisted photocatalysis of dicamba at (a) low (3.3 to 6.0) and (b) high initial pH levels (7.5 to 11.3).

dicamba

pH 5.3

Time (min)	x 10^{-5} M
0	2.17
2	1.47
4	1.07
6	0.69
10	0.36

pH 4.5

4.5	
Time (min)	x 10^{-5} M
0	2.18
2	1.61
4	1.15
6	0.84
10	0.47
15	0.213

pH 6

Time (min)	x 10^{-5} M
0	2.2
2	1.42
4	1.02
6	0.63
10.5	0.29

pH 3.3

Time (min)	x 10^{-5} M
0	2.17
3	1.71
6	1.17
9	0.93
12	0.750
15	0.52

pH 7.5

Time (min)	x 10^{-5} M
0	2.20
2	1.50
4	1.02
6	0.72
10	0.39

pH 10.1

Time (min)	x 10^{-5} M
0	2.17
4	1.30
8	0.79
12	0.52
16	0.32

pH 11.3

Time (min)	x 10^{-5} M
0	2.19
4	1.60
10	1.11
15	0.79
20	0.52

pH 8.9

Time (min)	x 10^{-5} M
0	2.2
2	1.54
4	1.11
6	0.82
8	0.61
12	0.32

Data for Figure 3.14. The variation of protonated ion intensity of alachlor and the reaction intermediates during the alachlor photocatalysis, where the initial pH level is 6.

Time	270	270	258	244	242	212	179.7	162.4	252	286
0	1.2E+06	1.5E+06								
6.5	7.1E+05	8.5E+05	6.0E+05	4.7E+05	8.6E+05	4.0E+05	3.1E+05	2.0E+05	3.5E+05	8.2E+05
10.5	5.3E+05	6.4E+05	6.6E+05	4.7E+05	5.9E+05	3.3E+05	4.0E+05	3.2E+05	3.7E+05	5.8E+05
20	2.2E+05	2.6E+05	4.0E+05	3.0E+05	5.0E+04	2.0E+05	4.1E+05	3.0E+05		1.2E+05
35							5.1E+05	3.5E+05		
51.5							5.2E+05	3.6E+05		
72							4.0E+05	3.8E+05		
96.5							2.0E+05	3.8E+05		
135										

Data for Figure 3.16 The variation of protonated ion intensity of alachlor, the reaction intermediates and end products during the H2O2-assisted photocatalysis at 300 nm, where the [H2O2] is 4.94 mmol/L and the initial pH level is 6.

Time	82.8	60	100	198	212	219	228	242
0								
1.5	9.2E+05	7.7E+05	3.0E+05	3.5E+05	1.5E+05	1.0E+06	6.7E+05	1.4E+06
3	1.5E+06	1.3E+06	6.6E+05	1.0E+06	4.5E+05	1.1E+06	1.0E+06	1.9E+06
4.5	1.8E+06	1.5E+06	1.8E+06	1.8E+06	6.0E+05	9.8E+05	1.1E+06	9.0E+05
20	3.1E+06	2.0E+06	3.1E+06	2.6E+06	4.1E+05		6.5E+05	5.5E+05
35	4.4E+06	2.5E+06	4.4E+06	2.9E+06	2.2E+05		2.0E+05	2.0E+05
51	4.7E+06	3.1E+06	4.9E+06	3.0E+06			1.0E+05	5.0E+04
70	6.2E+06	3.0E+06	5.2E+06	2.7E+06				
95	6.6E+06	3.1E+06	5.5E+06	2.5E+06				

Time	258	270	144	216	238	244	252	286
0		2.0E+06						
1.5	5.8E+05	1.8E+06	2.0E+05	5.0E+05	1.1E+06	2.9E+05	1.1E+06	6.9E+05
3	1.9E+06	1.1E+06	5.5E+05	7.0E+05	1.5E+06	6.5E+05	1.3E+06	1.1E+06
4.5	1.1E+06	5.0E+05	5.6E+05	6.2E+05	2.5E+06	2.5E+05	1.0E+06	5.1E+05
20	5.5E+05		5.8E+05	5.1E+05	1.7E+06	2.0E+05		
35	0.0E+00		6.0E+05	4.0E+05	1.0E+06	1.4E+05		
51			7.0E+05	3.5E+05	5.0E+05			
70			9.0E+05					
95			9.0E+05					

Data for Figure 3.17 Comparison of the photocatalytic decay of alachlor and TOC at 300 nm, where the $[H_2O_2]$ is 4.94 mmol/L and the initial pH level is 6.

Time (min)	ln t	TOC(mg/L)		TOC/TOCo
0	0.00	4.02		1.00
1.5	0.41	4.02		1.00
3	1.10	4.01		1.00
4.5	1.50	3.78		0.95
10	2.30	3.46		0.87
20	3.00	3.15		0.79
35	3.56	2.19		0.55
51	3.93	1.58		0.40
70	4.25	1.16		0.29
95	4.55	0.49		0.12